Measurement 243 (2025) 116355

Contents lists available at ScienceDirect

Measurement

journal homepage: www.elsevier.com/locate/measurement

Ann-based predictive model of geometrical deviations in dry turning of AA7075 (Al-Zn) alloy

F.J. Trujillo [a,*], S. Martín-Béjar [a], F. Bañón [a], T. Andersson [b], L. Sevilla [a]

[a] Department of Civil, Materials and Manufacturing Engineering, EII, University of Malaga, 29071 Malaga, Spain
[b] School of Engineering Science, University of Skövde, Högskolevägen 541 28, Skövde, Sweden

ARTICLE INFO

Keywords:
Light alloys
Sustainable machining
Surface integrity
Artificial neural networks
Machine learning

ABSTRACT

This work presents the use of a shallow feedforward artificial neural network (ANN) to develop a prediction model for geometrical deviations in the dry turning of the AA7075 (Al-Zn) alloy. The study focuses on the influence of cutting speed and feed on the arithmetic mean roughness, straightness, and circular runout of cylindrical specimens. The main novelty of this ANN-based model compared to traditional models lies in the simultaneous consideration of geometrical variables at macro and micro scales. The analysis showed that feed was the most influential variable, particularly at higher values, whereas cutting speed had a lesser impact. For all three analysed output variables, the optimal results were achieved by combining low feed and high cutting speed values. The proposed ANN model showed a reasonable adjusted R^2 value for all the variables, ranging from 0.87 to 0.97. The ANN performance was compared with other regression models, providing a better fit to the experimental data for all the output variables analysed. Testing of the ANN on additional data not included in the training and validation set confirmed its practical usefulness for predicting geometrical deviations under the studied cutting conditions.

1. Introduction

Currently, the aeronautical sector is prioritizing sustainability and energy efficiency as key objectives [1]. A significant goal for 2050 is to reduce emissions of harmful gases, such as CO_2 and NO_x, by 75 % to 95 % relative to levels recorded in 2000, underscoring the industry's commitment to environmental stewardship and operational improvements [2]. In this regard, the materials utilised in aircraft manufacturing play a crucial role in achieving these objectives. Light alloys, such as aluminum and titanium alloys, are predominantly used in the manufacture of structural components due to their favourable properties [3,4]. These alloys can be utilised as standalone materials or in combination with other materials, such as reinforced polymer matrix composites, to create laminated composites [5]. Wrought and cast aluminium alloys are employed in the fabrication of a diverse array of components utilized in the construction of aircraft. Cast aluminium alloys are a cost-effective solution for complex shapes, yet they exhibit inferior mechanical properties compared to wrought alloys. Consequently, they are best suited for non-critical components. Wrought aluminium alloys, renowned for their exceptional mechanical properties due to the plastic forming process they undergo [6], are selected for crucial airframe structural components (ribs, shear webs and wing tension structures, among others) that necessitate stringent mechanical properties (fatigue life, tensile and compressive strength) [7]. Series 2xxx and 7xxx aluminum alloys are preferred for their specific advantages in fracture toughness, fatigue behaviour, stress corrosion and cracking resistance [8].

Machining represents one of the most frequently employed manufacturing processes in the production of these components [9]. The production of final component geometries through machining processes involves mechanical, thermal, and chemical loads, along with their interactions. These processes can cause surface damage at both macroscopic and microscopic scales due to material removal mechanisms. These alterations of the surface include changes in surface topography and metallurgical, mechanical and chemical properties. These changes are collectively referred to as surface integrity [10]. The functional performance characteristics of manufactured components are adversely affected by poor surface integrity, which can lead to issues such as creep reduced corrosion and wear resistance or poor fatigue behaviour [11]. This is especially critical when machining light alloys under dry

* Corresponding author.
E-mail addresses: trujillov@uma.es (F.J. Trujillo), smartinb@uma.es (S. Martín-Béjar), fermin.banon@uma.es (F. Bañón), tobias.andersson@his.se (T. Andersson), lsevilla@uma.es (L. Sevilla).

https://doi.org/10.1016/j.measurement.2024.116355
Received 13 May 2024; Received in revised form 14 November 2024; Accepted 29 November 2024
Available online 30 November 2024

conditions. The severity of these modifications strongly depends on the machining inputs, such as lubrication, the cutting parameters or the tool wear, among others [12]. Due to environmental reasons, the current trend is to carry out these processes in a sustainable way, eliminating polluting agents from the production process, such as cutting fluids (dry machining) [13].

Although light alloys used in aeronautics and the automotive industry, such as aluminium and magnesium alloys (among others), are classified as materials with good machinability, the machining operations that involve them present several challenges. Aluminum alloys tend to be soft and sticky, which can lead to indirect adhesion tool wear in the cutting edge (built-up edge, BUE) and on the tool rake face (built-up layer, BUL) [14,15]. This material grows progressively until it reaches a limit value, breaking off and generating instabilities in the process. All of this can negatively affect the surface quality of the machined part. Additionally, chip morphology control is another relevant aspect to consider. The high ductility of these alloys tends to generate continuous chips, since the shear breaking limit of the material is not reached, creating chip nests that become entangled in the part and the machine tool, causing unnecessary stops in the process [5,16]. Magnesium alloys, also prevalent in aerospace and automotive applications for their lightweight properties, pose different machinability issues. While these alloys are easier to cut due to their lower hardness compared to aluminum alloys, they are highly flammable, especially in the form of chips and dust during machining operations. This characteristic necessitates stringent safety measures to prevent and manage fires, complicating the machining process. Furthermore, magnesium's reactivity with other materials can lead to galvanic corrosion when in contact with dissimilar metals, requiring careful selection of machining environments and tool materials [17,18].

Currently, there is a substantial body of knowledge regarding the sustainable machining of lightweight alloys utilized in the aerospace industry. In this context, the most extensively studied variables pertain to surface integrity, encompassing geometrical variables at both the microscale (roughness profile) and the macroscale (dimensional and geometrical tolerances). Additionally, the physicochemical properties of the surface are of significant interest [19]. A common method of disseminating this knowledge to the industrial sector is to provide straightforward equations that can be used to predict the value of machining output variables as a function of input variables, mainly the cutting parameters (cutting speed, v_c; feed rate, f; and depth of cut, a_p).

Regarding the roughness profile, a great variety of equations can be found in the literature, mainly potential and polynomial type equations, which allow obtaining parameters such as the arithmetic average of roughness profile (Ra) or the maximum height of roughness profile (Rz) as a function of the cutting parameters. Salguero et al. studied the influence of v_c and f on Ra in the turning of the AA2050 (Al-Cu-Li) alloy under dry conditions [20]. Several models (linear, quadratic, and potential model) were proposed to predict Ra. The potential model demonstrated the most accurate correlation with the experimental data. The model showed a statistically significant correlation between Ra and f, with Ra exhibiting a general tendency to increase with an increase in f. The impact of v_c was less significant, as Ra tends to decrease with an increase in v_c. In [21], a similar study was conducted in the dry machining of AA7075 (Al-Zn). The results indicate that f had the greatest influence, while v_c and a_p showed a lower level of influence. A potential model was developed with an adjusted R-squared (R^2) value of 0.75. De Agustina et al. studied the influence of the cutting parameters, the tool nose radius and the machined length on Ra in the dry turning of AA7075 (Al-Zn) alloy [22]. The analysis of variance (ANOVA) showed that the most influential parameter was f and the interaction between the nose radius and f. In addition, a predictive polynomial model based on the cutting forces was developed. According to the R-squared value, the model explained a 64.473 % of variability on Ra. Sebastian et al. analysed the influence of the cutting parameters in the dry machining of AA2024 (Al-Cu) alloy [23]. A potential parametric equation was developed that can be used to predict the surface quality of the machined parts as a function of v_c and f.

Conversely, despite the significance of geometric tolerances on coupling parts and the elevated quality standards in the aerospace industry about this matter, studies that focus on the analysis of macro-geometrical tolerances are relatively scarce. Some models have been developed (potential and exponential type) in the sustainable machining of aluminum alloys for aircraft use. These models allow obtaining some form deviations (straightness, parallelism, roundness, circular runout or cylindricity) as a function of v_c and f. Sánchez et al. studied the specimen straightness in the turning of AA2024 (Al-Cu) alloy. A parametric model to predict the straightness, based on f and v_c, was developed [24]. The proposed potential model showed good agreement with experimental data, with differences between experimental and theoretical values not exceeding 10 %. The same author developed several exponential models to predict the straightness, parallelism and roundness as a in the turning of AA2024 (Al-Cu) cylindrical bars under dry conditions, obtaining a reasonable fit (R^2 about 0.75–0.81) [25]. In [26], a series of cutting speed-feed coupled models were developed for several geometrical deviations in the dry turning of AA7075 (Al-Zn) alloy, in low slenderness specimens. The regression models generated were of exponential type, with R^2 between 0.63 and 0.71. The authors concluded that the geometrical deviations analysed exhibited a lower sensitivity to change with the cutting parameters than Ra, with f identified as the most influential factor. Martín-Béjar et al., in [27], studied the cutting parameters influence on form deviations in dry machining of AA7075 (Al-Zn) alloy. Feed was revealed as the most influential parameter in most of the geometrical deviations analysed. In addition, predictive models (potential type) were proposed for the form deviations as a function of the cutting parameters, showing a reasonable fit (R^2 about 0.75–0.80).

As the literature review shows, these models are typically focused on a single output variable (single-objective optimisation). A limited number of models are capable of simultaneously involving several output variables (multi-objective optimisation), due to the inherent complexity of machining. However, the significant advancements in computational methods in recent years have enabled the development of autonomous learning algorithms capable of adjusting machining parameters to achieve a specific target [28]. The utilisation of these algorithms constitutes a key aspect of the concept of "intelligent machining". This encompasses the creation of interactions with a range of systems (big data, controllers, tools, sensors or cloud computing, among others) [29]. There exists a diverse array of algorithms designed to tackle regression problems, each suited to different kinds of data and complexities. These include Linear Regression, Polynomial Regression, Ridge Regression, Lasso Regression, Elastic Net, Decision Tree Regression, Random Forest Regression, Gradient Boosting Machines, Support Vector Regression (SVR), and various forms of Artificial Neural Networks (ANN). Among these, ANN is one of the most widely used due to its exceptional ability to model complex and nonlinear relationships between variables, as occurs in machining processes. This capability stems from ANNs layered structure, which enables the algorithm to learn intricate patterns and dependencies directly from data, without explicit programming for feature interaction. Additionally, ANNs adaptability allows it to perform well on large and diverse datasets, making it highly effective across many domains and applications [30,31]. In this context, ANNs represent one of the most frequently employed algorithms for modelling machining operations [32–34]. Several machining aspects are covered by this matter [35], such as monitoring (tool wear, temperature, cutting forces, chattering, or energy consumption) [36,37], surface quality control [38] or modelling (obtaining regression models to predict the outputs variables as a function of the input variables) [39], among others.

Focusing on the machining of light aluminium alloys, numerous works in the literature use ANN for surface roughness analysis. Aljinović et al. investigated the influence of v_c, a_p and f on Ra, as well as the power consumption in the longitudinal turning process of AA2011 (Al-Cu)

alloy [40]. The prediction accuracy of two methods, Response Surface Methodology (RSM) and Artificial Neural Network (ANN), was analysed. The surface roughness quality was negatively affected by the feed rate, which was the most influential variable. The use of ANN provided superior predictions for surface roughness. However, no notable discrepancy was observed in the mean error values obtained by ANN and RSM in terms of power prediction.

Muñoz-Escalona et al. studied the effectiveness of various ANNs in predicting surface roughness in AA7075 (Al-Zn) alloy after high-speed face milling [41]. The ANNs tested included radial base neural networks (RBNN), feedforward neural networks (FNN), and generalized regression neural networks (GRNN). The correlation between the cutting parameters, the chip geometry and the surface quality was analysed using the Pearson correlation coefficient. The study revealed a robust correlation between chip thickness and surface roughness, with v_c emerging as the second most influential factor. The effectiveness of artificial neural networks in predicting surface roughness under the applied conditions was demonstrated, with FNN performing the best among the tested networks (lower square error percentage).

Fang et al. developed two ANN models, Multi-Layer Perceptron (MLP) and Radial Basis Function (RBF), for predicting surface roughness in machining AA2024 (Al-Cu) alloy [42]. The models were trained and tested using data collected from force and vibration sensors, and the inputs included cutting speed, feed rate to tool-edge radius ratio, cutting forces, and cutting vibrations. The MLP model showed higher accuracy ($MSE = 0.285$ %) in predicting *Ra* compared to the RBF model ($MSE =$ 0.830 %).

Al-Ani compared the predictive performance of ANN and response surface methodology (RSM) models in predicting surface roughness in the turning process of AA96061 (Al-Mg-Si) [43]. The results showed that cutting speed was the most influential cutting parameter on *Ra*. This is due to their high Si content that results in abrasive tool wear, which in turn affects surface quality more significantly than feed rate. Furthermore, the ANN model showed higher accuracy and better predictive performance compared to the RSM model, indicating its ability to learn and predict complex patterns and relationships.

Kumar et al. conducted a study on the impact of cutting parameters on surface roughness during the dry turning of UNS A97075 hard ceramic composite and hybrid composite [44]. The study found that the surface roughness of the hybrid composite was lower than that of the hard ceramic composite. The primary contributor to surface roughness was found to be the feed rate. The best results were achieved at a low feed rate. The surface roughness was significantly affected by the relationship between feed rate and cutting speed. The best results were achieved by combining low feeds with high cutting speeds. To develop a prediction model, both RSM and ANN were used. The RSM model was found to be more accurate than the ANN model.

Arunkumar et al. investigated the impact of various machining parameters on surface roughness of Al-Si (LM6) alloy, employing a feedforward neural network to predict outcomes based on input variables like cutting speed, feed rate, and coolant flow rate. The optimal architectural determination necessitated a considerable degree of trial and error, resulting in an estimated 10 % margin of inaccuracy in the *Ra* predictions. The findings indicate that the trained neural network can effectively map these inputs to desired outputs, thus facilitating better decision-making in machining operations [45].

Kosarac et al. analysed the use of ANNs to predict the arithmetic mean roughness (*Ra*) in machining processes, specifically for AA7075 aluminum alloy. It highlights the challenges of traditional analytical methods for determining *Ra* due to their complexity, advocating for empirical models instead. A total of 27 experiments were conducted using a Taguchi methodology, reducing the initial 81 experiments through an orthogonal design. Several ANN architectures and algorithms for training. The results indicate that the best performance was achieved using backpropagation multilayer feedforward neural networks with the BR (Bayesian Regularization) algorithm for training. The paper also discusses the evaluation of network performance by comparing predicted *Ra* values with experimentally obtained values, showing a good fit with *R* values of 0.9758. The study demonstrates that ANNs can effectively be trained with small datasets, achieving reliable predictions for surface roughness [46].

Eser et al. focused on improving mathematical and predictive models for estimating surface roughness (*Ra*) in milling AA6061 alloy using carbide cutting tools under dry conditions. Artificial Neural Networks (ANN) and Response Surface Methodology (RSM) were compared, evaluating their effectiveness in predicting surface roughness. Key input parameters analysed include cutting speed, depth of cut, and feed rate. Statistical analysis through ANOVA confirmed the significance of these parameters. The study highlights that the depth of cut is the most significant factor affecting surface roughness, contributing 35.48 % to the overall impact, followed by cutting speed and feed rate. The ANN model was trained using various algorithms, with the standard backpropagation algorithm identified as the most effective for this study. The findings suggest that both ANN ($R^2 = 95.6$) and RSM ($R^2 = 99.9$) are valuable for estimating surface roughness, with RSM demonstrating slightly better stability in predictions [47].

Other research focuses on the monitoring of cutting forces, tool wear or energy consumption. Efkolidis et al. investigated the development of predictive models for thrust force (F_z) and cutting torque (M_z) in drilling AA6082 (Al-Mg-Si) alloy using ANN [48]. The models were developed based on a three-level full factorial design of experiments, considering cutting speed, feed rate, and tool diameter as process parameters. The ANN models achieved high accuracy in predicting thrust force (4 % error) and cutting torque (4.5 % error), with correlation coefficients (*R*) of 0.97 and 0.99, respectively. The study highlights the suitability of ANN models for accurately predicting thrust force and cutting torque in drilling operations, promoting better machining quality. Yau et al. developed a machine learning model that predicts tool wear in milling; Depth of cut, feed rate, material, and AC spindle motor current were selected to predict the evolution of the flank wear parameter (*VB*). An ANN model is proposed, integrating automatic hyperparameter tuning and transfer learning. This model utilizes features extracted from a single type of sensor signal, enhancing training efficiency. The architecture combines Inception and DenseNet, which improves feature reuse and prevents issues like gradient vanishing. Layer Normalization is also employed to boost computational efficiency. The model performance is evaluated against traditional models using metrics such as Mean Absolute Error (*MAE*), Root Mean Square Error (*RMSE*), and Coefficient of Determination (R^2). The proposed model demonstrates superior accuracy, achieving a *MAE* of 0.03527 and an R^2 of 0.9611, outperforming common models like Random Forest by significant margins [49]. Wiciak et al. explored the use of multilayer perceptron networks to predict tool wear during milling of Aluminium Matrix Composite (AMC) with 10 % SiC content, using vibration acceleration and cutting forces as input signals [50]. The developed models were analyzed to select the most efficient ones and assess the quality of tool wear prediction. Veeranaath et al. studied the influence of the cutting parameters on surface quality and tool wear in the machining Ti6Al4V alloy. The study employs the L25 Taguchi array to analyze the effects of varying the cutting speed, feed and depth of cut at five levels, aiming to optimize surface roughness and tool wear. The paper also discusses the development of regression and artificial neural network (ANN) models to predict output responses based on input factors, demonstrating the effectiveness of ANN in simulating the cutting process [51].

Kulkarni et al. developed a mathematical model for the prediction of surface quality, cutting forces and tool life in the turning of Inconel 718 alloy under Minimum Quantity Lubrication (MQL) conditions. Artificial neural networks (ANN) and adaptive neuro-fuzzy inference systems (ANFIS) were employed for the purpose of predicting these variables. The experimental parameters included cutting speed, feed and depth of cut. A total of 15 experiments were conducted. The results indicated that the ANN and ANFIS models accurately predicted the cutting force,

surface roughness and tool life, with an average prediction error of less than 15 %. The ANFIS model was shown to be more accurate in predicting surface roughness and tool life, whereas the ANN was more accurate in predicting the cutting forces. The authors also highlighted that performance improved with iterative training and parameter fine-tuning [52].

Bousnina et al. investigated the gap between existing machining models and their application in optimizing tool paths, energy consumption, and costs during the milling of the 2017A (Al-Cu) alloy. A hybrid approach combining Genetic Algorithm-Artificial Neural Network (GA-ANN) and Response Surface Methodology (RSM) is proposed to predict surface quality, cost, and energy consumption. The study reveals significant improvements in energy consumption and costs, with the depth of cut being the most influential factor. The GA-ANN model outperformed the RSM model, achieving reductions of 90.91 % in total energy, 96.55 % in cost, and 40.18 % in surface roughness. The potential of advanced predictive models in improving machining efficiency and reducing costs in the metal processing industry is also highlighted [53].

Regarding the mechanical properties related to surface integrity, few studies have been found that analyse these properties using ANN. Reza et al. developed an algorithm based on ANN to predict the fatigue life of AA7075 (Al-Zn) and AA92024 (Al-Cu) alloys [54]. The algorithm uses input variables such as yield strength, ultimate tensile strength, depth of cut, cutting speed, feed rate, and applied cyclic stress to predict surface roughness and the number of cycles to failure. The results obtained from the ANN predictions were compared with experimental values, showing good agreement in the case of the surface roughness prediction. However, the direct algorithm for predicting fatigue life was unable to accurately estimate the cyclic life based solely on machining process parameters. The fit of the experimental data to the predicted value was only in the range of 60–80 %.

With respect to macrogeometrical deviations, only a limited number of studies have been identified that address the use of ANNs in obtaining predictive models, despite the importance of this topic. Kalos et al. [55] studied the application of ANNs to control roundness in dry turning processes of cylindrical bars, showing the effectiveness of back propagation over quick propagation algorithms. Du et al. [56] investigated the potential of machine learning techniques in accurately predicting product quality parameters in hard turning processes. The use of ANN showed high prediction accuracy for roughness profile and roundness, using spindle vibration and cutting force as inputs. Jeffrey at al. studied the prediction of circularity and cylindricity in O1 steel during CNC turning operations, utilizing ANNs for analysis. A feed-forward neural network with a 3–10-2 configuration was identified as the optimal model. The authors employed the Lavenberg-Marquart algorithm for training the ANN. The results demonstrated a high regression value of 0.98, indicating strong predictive performance. The study highlights the effectiveness of the backpropagation learning algorithm in establishing a reliable model, with low average error rates of 0.2 and 2 %. The research also integrates Taguchi Topsis methods to enhance the accuracy of the output responses, showcasing a comprehensive approach to optimizing machining [57].

In summary, the use of ANNs to predict the surface quality in the machining of light aluminium alloys has been extensively studied, showing good results in its application. With respect to the physic-chemical properties of the surface and form deviation, these studies are scarce. Therefore, in this work, a study was conducted to examine the efficacy of ANNs in developing regression models for geometrical deviations, specifically surface roughness and form deviations, in the dry turning of AA7075 (Al-Zn) cylindrical specimens. In particular, the surface quality obtained as a function of the cutting the cutting parameters has been analysed. The parameter selected to characterize the roughness profile quality was the arithmetic mean roughness (*Ra*). The straightness (*STR*) and circular runout (*CRO*) of the specimens were also controlled. The main novelty of this study lies in obtaining a regression model of the experimental results that considers several geometrical variables from both micro and macro scales simultaneously. Macro and microgeometric scales are closely related, but there is no model in the literature that integrates their prediction. ANNs are based on feature-based learning, so they have the ability to learn important features of the data automatically, being less sensitive to noise and ambiguity in the input data. The inclusion of all output variables (macro and micro) makes the model depend on the results obtained at both scales simultaneously, during the iteration process of the algorithm. Finally, the results of the ANN model were compared with those obtained by other models in previous research on this alloy (under similar cutting conditions). The proposed model could be of significant benefit at an industrial level, as it can provide the geometric deviation values as a function of the applied cutting parameters.

2. Experimental methodology

Machining tests were conducted on cylindrical bars of the AA7075-T6 (Al-Zn) aeronautical aluminium alloy. Table 1 shows the chemical composition of the tested alloy.

The machining tests were conducted on turning center, EMCOTURN E45 (Fig. 1a). Cylindrical specimens ranging from 40 to 70 mm in diameter (*D*) and 150 mm in length (*L*) were utilized (Fig. 1b). An uncoated WC-Co rhombic insert with ISO reference DCGT11T308 was used as the tool (Fig. 1c). This tool is recommended by the manufacturer for machining this type of alloy. To guarantee the maintenance of consistent initial conditions, a new tool was employed for each individual test. All tests were conducted under dry conditions.

Twelve turning tests were performed using the input values shown in Table 2. These values fall within the recommended range for machining this alloy, as recommended by the tool manufacturer. It is important to note that aluminum alloys are not usually machined at low v_c (40–80 m/min). However, these values are common when it is combined with other materials, such as Titanium alloys or CFRP [27].

After each machining test, the micro and macrogeometrical deviations of the specimens were controlled (Fig. 2). The roughness profile was obtained using a roughness tester, Mitutoyo Surftest SJ-210 model (Fig. 2a). *Ra* was selected as the parameter to characterise the surface quality. The specimens were measured at six equidistant generatrix (*G1-G6*), 60° apart, as shown in Fig. 2c and d. The cutoff and evaluation length were selected according to the ISO 21920–2:2021 standard [58]. These measurements were repeated at six sections (*S1-S6*). The result of *Ra* in each generatrix was expressed as the mean value in these sections.

A form measuring machine (Accretech RONDCOM NEX model, detector E-DT-R120A, Stylus EM46000-S302) was used to measure the straightness (*STR*) and the circular runout (*CRO*) of each specimen (Fig. 2b). *STR* was measured at six generatrix, *G1-G6* (Fig. 2c and d). *CRO* was measured along the specimen in several sections (*S1-S6*), 25 mm apart (Fig. 2c). In this way, a total of 72 experimental data were obtained for *Ra*, *STR* and *CRO*.

The procedure for obtaining *STR* and *CRO* is outlined in Fig. 3. The STR represents the distance Dmax − Dmin. The CRO is the difference between the radii of two concentric circumferences (Rmax − Rmin) that contain the profile. The centre of these circumferences coincides with the rotation centre of the workpiece.

A supervised shallow feedforward ANN was used to obtain a prediction model of *Ra*, *STR* and *CRO* as a function of f and v_c. Fig. 4a illustrates the structure of this type of ANN, which is characterised by a single hidden layer. It is composed of several neurons (nodes) connected by synaptic links (weights) and arranged in layers. The architecture

Table 1
Chemical composition of the tested alloy (weight %).

Zn	Mg	Cu	Cr	Si	Mn	Al
6.02	2.61	1.86	0.18	0.09	0.06	Rest

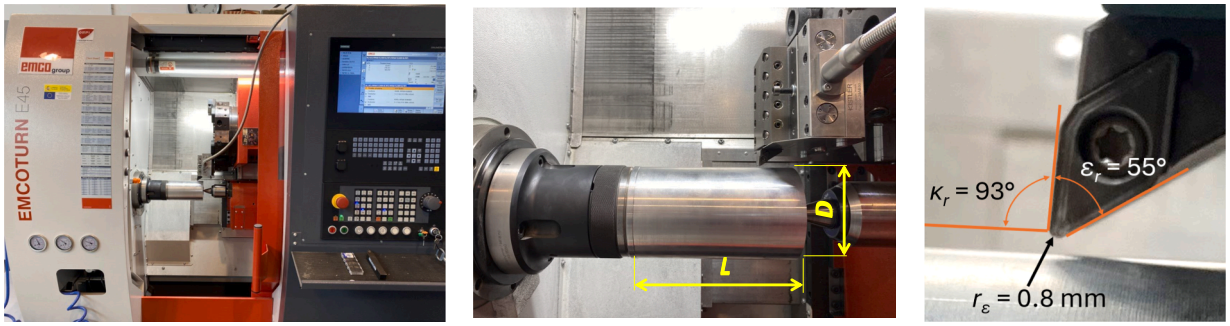

Fig. 1. (a) Turning Center EMCOTURN E45; (b) Specimen geometry (length, L; diameter, D); (c) Cutting tool (corner radius, r_ε; insert included angle, ε_r; Tool cutting edge angle, K_r).

Table 2
Tested values for the cutting parameters.

f [mm/rev]	v_c [m/min]	a_p [mm]
0.05	40	1
0.10	80	
0.20	150	
	200	

consists of nodes in each layer receiving forward connections from nodes in the previous layer. Each node processes information through the connection weights, as shown if Fig. 4b [60].

The output y_i (excitation) of a node (denoted by i) is computed as:

$$y_i = \varphi_i\left(\sum_{J=1}^{n_i} w_{ij}z_{ij} + b_i\right) \quad (1)$$

where n_i represents the total number of incoming connections, z_{ij} denotes the input, w_{ij} is the weight, b_i is the bias, and φ_i is the activation function at the i-th node.

Fig. 5a shows the architecture of the ANN implemented for this work, with two input variables and three output variables. Since the diameters (D_m, mm) of the specimens were different for each machining test, the feed rate (v_f, mm/min) and the rotational speed (n, rev/min) were used as input variables instead of f (mm/rev) and v_c (m/min). These variables can be related by Eq. (2) and (3). Expanding the value range of input variables for the ANN typically leads to improved performance [61].

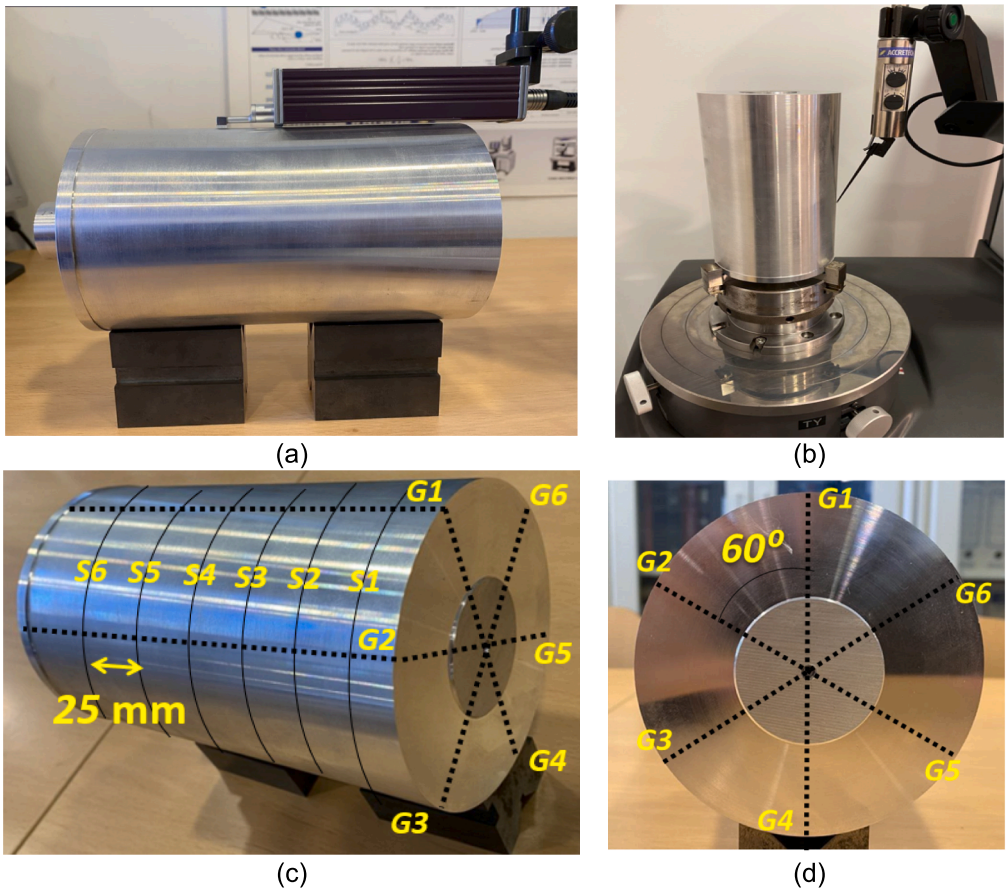

Fig. 2. Measurement setup: (a) Roughness tester; (b) Form measuring machine; (c) Generatrix and sections for measuring *Ra*, *STR* and *CRO*; (d) Specimen cross section.

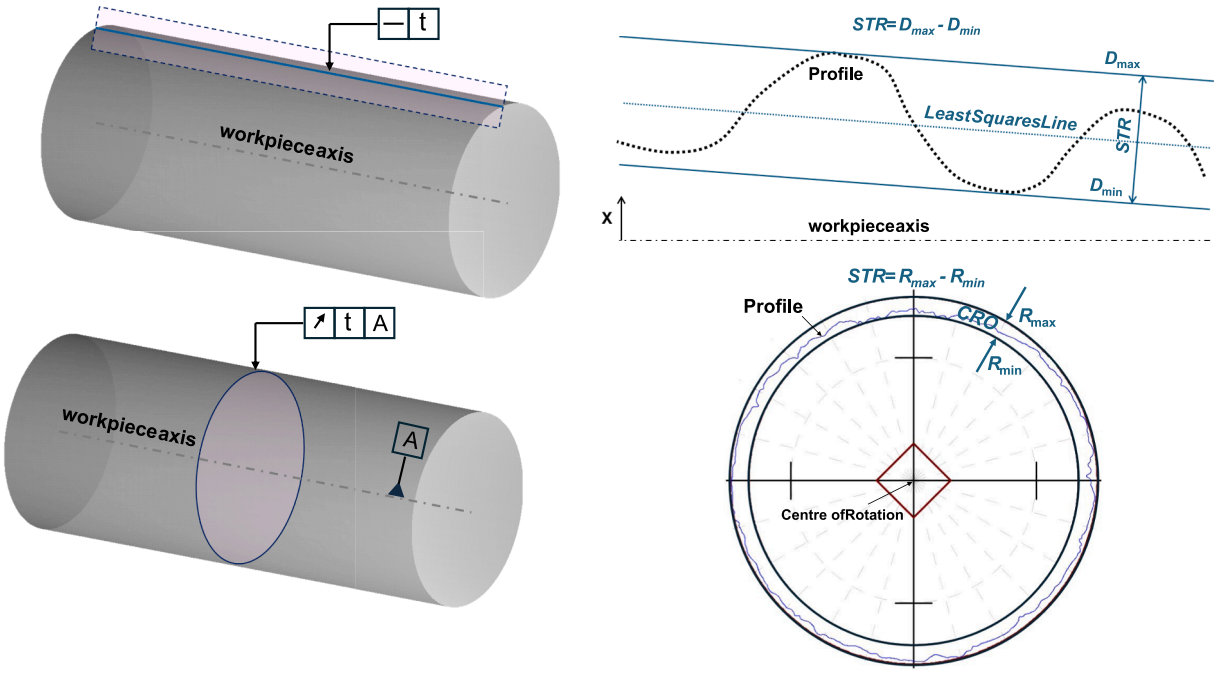

Fig. 3. Procedure for obtaining STR and CRO [59].

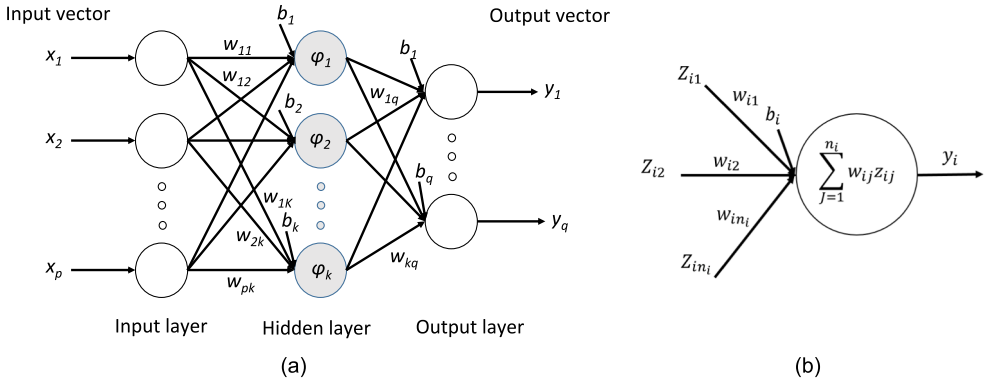

Fig. 4. A) General scheme of a shallow feedforward ANN; b) Node structure.

Although the transformation performed is not relevant from a technological point of view, it is useful from a computational point of view. Data transformation is a critical yet often overlooked preprocessing step in many data science pipelines. A right transformation can significantly improve the performance of the learning algorithm. Conversely, a wrong transformation can skew the data leading to worst results [62,63]. The output variables were *Ra*, *STR* and *CRO*. The activation function applied in the first stage to generate the output of the hidden neuron was a sigmoid function (Eq. (4), while a linear function (Eq. (5) was used in the second stage to generate the final outputs (Fig. 5b).

$$v_f = fn \tag{2}$$

$$v_c = \pi D n 10^{-3} \tag{3}$$

$$\varphi(x) = \frac{1}{1+e^{-x}} \tag{4}$$

$$\varphi(x) = x \tag{5}$$

The ANN has been implemented using Matlab and Simulink software. The software version used was Matlab-Simulink 23.2 (R2023b, Academic use). To train the ANN, several algorithms were employed: Levenberg-Marquardt (LM); Bayesian Regularization (BR); and Scaled Conjugate Gradient (SCG). These algorithms are suitable for the rapid training of small datasets [64]. In addition, BR helps to prevent overfitting by introducing regularization, while SCG offers a more memory-efficient approach. The performance of the ANN was compared for these algorithms, selecting the one that gave the best results. Out of the 72 experimental data collected for each output variable, 60 were used for training, while the remaining 12 were reserved for validation. To guarantee that the data used in the validation phase are representative for the experimental dataset, at least one experimental data for each combination of cutting parameters has been selected for the validation phase.

The initial stage of the study involved an analysis to identify the optimal number of neurons (*N*) required for the design of the ANN. This was done to prevent the occurrence of underfitting and overfitting. The ANN was tested for *N* values ranging from 1 to 20, with the Mean Squared Error (*MSE*) and the Root Mean Squared Error (*RMSE*) being used as performance parameters (Eqs. (6) and (7):

$$MSE = \frac{\sum_{t=1}^{T}(\hat{y}_t - y_t)^2}{T} \tag{6}$$

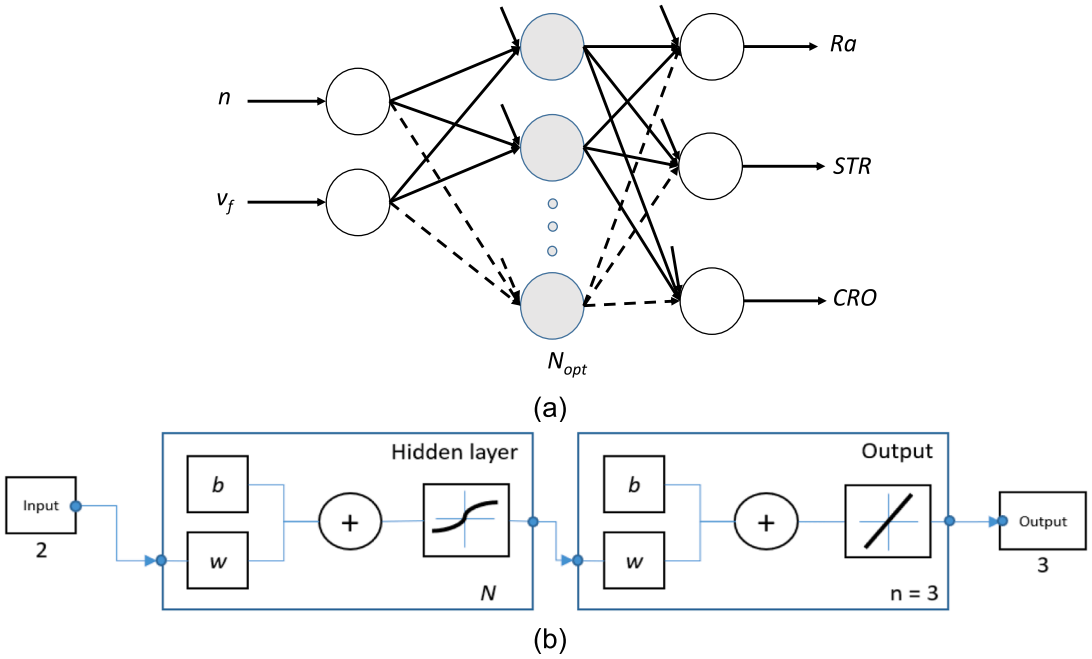

Fig. 5. ANN used to predict Ra, STR and CRO as a function of S and F: a) General scheme; b) Activation functions in the hidden and output layers.

$$RMSE = \sqrt{MSE} \tag{7}$$

where $\hat{y}_t$ are the predictions, y_t the experimental data and T the number of observations.

The optimal number of neurons (N_{opt}) was selected according to the lowest *MSE*. To achieve better ANN performance, the values of the used variables were normalized from 0 to 1 (Eq. (8) due to their different scales.

$$Y_{norm} = \frac{Y - \min(Y)}{\max(Y) - \min(Y)} \tag{8}$$

where Y_{norm} represents the normalized value (0–1) of Y (v_f, n, *Ra*, *STR* or *CRO*). The terms max(Y) and min(Y) are used to denote the maximum and minimum values of Y.

A manual deactivation of the default normalisation ("mapminmax") of the ANN has been performed, both on input and output variables, by means of the matlab functions: *net.input.processFcns* = {}; *net.output.*

Table 3
Experimental dataset.

v_c(m/min)	f (mm/r)	v_f (mm/min)	n (rpm)	D(mm)	*Ra* (μm) *S1*	*S2*	*S3*	*S4*	*S5*	*S6*
40	0.05	11	227	56.2	0.62	0.62	0.55	0.55	0.43	0.40
40	0.10	29	293	43.4	0.71	0.76	0.74	0.56	0.58	0.65
40	0.20	43	217	58.7	1.81	1.94	2.41	2.17	2.00	2.17
80	0.05	28	556	45.8	0.57	0.57	0.45	0.42	0.34	0.31
80	0.10	42	417	61.0	0.51	0.69	0.64	0.56	0.52	0.50
80	0.20	106	528	48.2	2.18	2.13	2.07	2.08	2.07	2.04
150	0.05	47	947	50.4	0.77	0.67	0.62	0.53	0.47	0.40
150	0.10	75	753	63.4	0.83	0.81	0.79	0.66	0.60	0.55
150	0.20	182	908	52.6	1.50	1.50	1.45	1.40	1.43	1.39
200	0.05	49	970	65.6	0.74	0.75	0.67	0.58	0.51	0.50
200	0.10	94	936	68.0	0.58	0.56	0.55	0.55	0.53	0.52
200	0.20	233	1164	54.7	1.49	1.50	1.48	1.48	1.51	1.49

v_c(m/min)	f (mm/r)	v_f (mm/min)	n (rpm)	D (mm)	*STR*(μm)						*CRO*(μm)					
					G1	*G2*	*G3*	*G4*	*G5*	*G6*	*S1*	*S2*	*S3*	*S4*	*S5*	*S6*
40	0.05	11	227	56.2	13.57	13.68	12.63	13.15	13.20	13.40	8.57	9.04	8.53	7.72	6.12	6.50
40	0.10	29	293	43.4	19.62	17.03	16.80	18.22	17.35	18.83	9.07	11.11	10.50	12.30	10.85	11.40
40	0.20	43	217	58.7	14.31	16.13	18.05	16.15	17.52	16.75	13.73	11.72	11.32	10.64	10.38	9.77
80	0.05	28	556	45.8	14.84	15.15	16.91	15.48	16.38	15.75	12.10	11.39	12.05	9.15	10.81	9.89
80	0.10	42	417	61.0	14.50	17.25	15.54	14.16	15.38	14.98	14.10	12.83	13.20	12.88	9.85	11.44
80	0.20	106	528	48.2	12.85	13.34	13.65	16.92	14.05	13.90	15.24	14.98	13.81	14.62	15.86	14.79
150	0.05	47	947	50.4	9.69	10.22	11.40	10.43	11.32	10.87	7.60	5.69	5.52	7.69	7.06	7.14
150	0.10	75	753	63.4	11.07	11.79	11.96	11.59	12.01	11.36	11.55	12.32	12.79	13.25	10.08	12.83
150	0.20	182	908	52.6	19.66	19.03	20.11	21.89	21.03	20.42	16.11	14.95	17.33	16.09	18.40	17.22
200	0.05	49	970	65.6	11.37	10.59	11.19	13.27	13.98	12.21	8.69	9.52	8.40	6.54	5.68	3.74
200	0.10	94	936	68.0	15.68	14.60	16.22	14.07	15.33	14.95	15.40	11.01	12.05	5.03	6.00	8.00
200	0.20	233	1164	54.7	22.18	21.99	19.10	20.33	18.23	21.35	22.07	21.25	20.89	23.56	21.08	21.93

processFcns = {}; This allows manual control of the type of normalisation used. This step has been generated externally to the network, to highlight the importance of the initial normalisation and processing of the data on the performance of the network.

Following training and validation, the ANN predictive model was integrated into a Simulink environment. Furthermore, its performance was tested using *Ra*, *STR*, and *CRO* values obtained from machining tests conducted with cutting parameters different from those used during the training and validation phases.

3. Results and discussion

Table 3 shows the experimental dataset obtained from the machining tests and measurements of micro and macrogeometrical deviations.

Fig. 6 shows the average of *Ra* as a function of *f*.

Ra ranges from a minimum of 0.31 μm ($f = 0.05$ mm/rev, $v_c = 80$ m/min) to a maximum of 2.41 μm ($f = 0.20$ mm/rev, $v_c = 40$ m/min). From $f = 0.05$ to 0.10 mm/rev, there was no significant variation in *Ra*, for both f and v_c. Only a slight increase with f was observed for most v_c tested, except for $v_c = 200$ m/min. However, a noticeable increase in *Ra* was shown from $f = 0.10$ to 0.20 mm/rev, regardless of v_c. For the low range of cutting speed (v_c) analysed (40–80 m/min), the *Ra* mean value was increased 3.6 times (from approximately 0.6 to 2.2 μm). The increase in *Ra* was 2.5 times higher at the high range of v_c (150–200 m/min) where it increased from about 0.6 to 1.5 μm. Therefore, it appears that f is the most influential cutting parameter. The mean value of *Ra* showed a general trend to increase with f, particularly from f = 0.10–0.20 mm/rev. However, v_c had a lower influence, only being significant for high values of f. When transitioning from the low range (40–80 m/min) to the high range (150–200 m/min) of v_c, *Ra* was reduced. The combination of low v_c and high f leads to the worst values. High f causes more pronounced marks on the machined surface and more material removal, which can generate chatter. Low v_c causes the appearance of material adhesion due to thermo-mechanical effects [65,66]. This type of indirect adhesive tool wear is enhanced by the total absence of cutting fluid during the process. The surface quality of the machined part is negatively affected by the combination of these effects [67]. Fig. 7 shows images of the tool rake face and chip obtained under favourable ($v_c = 80$ m/min; $f = 0.05$ mm/rev) and unfavourable ($v_c =$ 200 m/min; $f = 0.20$ mm/rev) cutting conditions. Under favourable conditions (Fig. 7a), less indirect adhesion tool wear is shown on the cutting edge (BUE, Built-Up Edge) and the rake face (BUL, Built-Up Layer). This tool wear is higher under unfavourable conditions (Fig. 7b), which can negatively affect the process stability (BUE and BUE detachment) and the surface quality of the workpiece. On the other hand, the chip generated in both cases are of a continuous type. However, a higher fragmentability is observed under favourable conditions. This allows a faster evacuation of the chip in the cutting edge and, therefore, of the heat generated. Under unfavourable conditions, the chip is more continuous, tending to generate chip nests that can negatively affect the surface quality of the machined part.

Fig. 8 displays the mean values of *STR* as a function of *f*. The range of *STR* varies from a minimum of 9.69 μm ($f = 0.05$ mm/rev and $v_c = 150$ m/min) to a maximum of 22.18 μm ($f = 0.20$ mm/rev, $v_c = 200$ m/min). For $f = 0.05$ to 0.10 mm/rev, an increase (15–40 %) of *STR* was observed for $v_c = 40$ and 200 m/min, whereas the *STR* remained almost constant for $v_c = 80$ and 150 m/min. From $f = 0.10$ to 0.20 mm/rev, the *STR* was increased significantly (close to 70 %) for $v_c = 150$ m/min. The increase was slightly lower (close to 33 %) for $v_c = 200$ m/min, whereas it remained practically constant for the low range of v_c (40–80 m/min). In contrast to *Ra*, where f was identified as the dominant cutting parameter, the influence of f on *STR* is more evident at high v_c ranges (150–200 m/min). Additionally, v_c has a less impact on *STR* than on *Ra*. The worst results were obtained by combining high values of f and v_c. Nevertheless, the influence of the cutting parameters was generally less pronounced than for *Ra*. Phenomena such as the appearance of indirect adhesion tool wear (BUL and BUE) or the morphology of chip generated (continuous or fragmented) affect more evidently at micro scale (height of peaks and valleys of the roughness profile) than at macro scale (where the roughness profile is filtered) [68,69]. High values of f can cause chatter, leading to negative effects on geometrical deviations. This is combined with the temperature increase that occurs when the v_c is increased, which affects tool wear and can lead to further expansion of the part [26]. A similar trend has been identified in the literature for this alloy in similar studies but applied to high slenderness parts [27]. Combining high values of f and v_c resulted in larger differences in those cases, due to the higher deflection of the part.

Fig. 9 plots the average for *CRO* as a function of *f*.

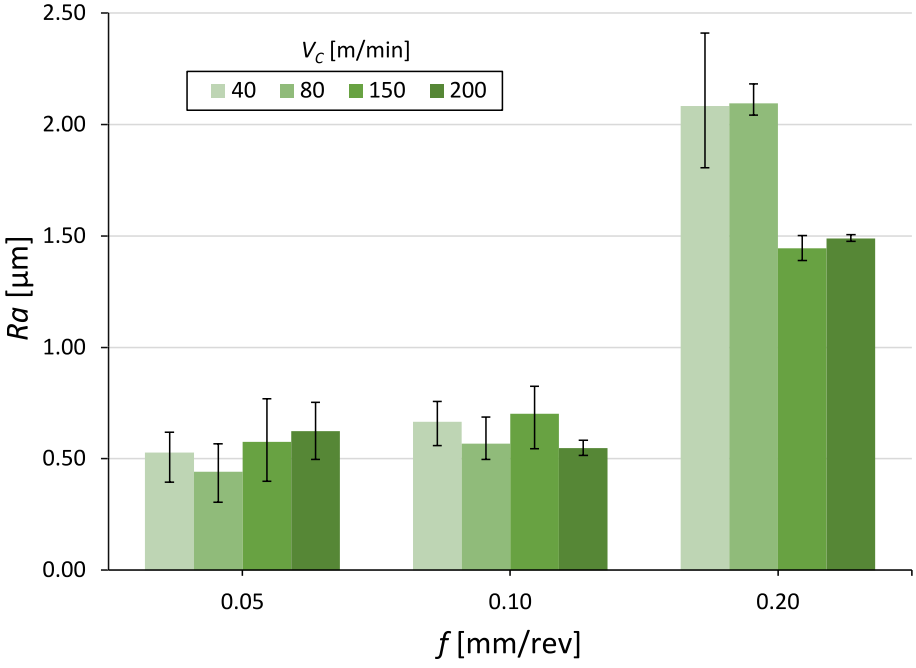

Fig. 6. Mean values of the arithmetic average of roughness profile (*Ra*) as a function of the feed rate (*f*), for each cutting speed (v_c).

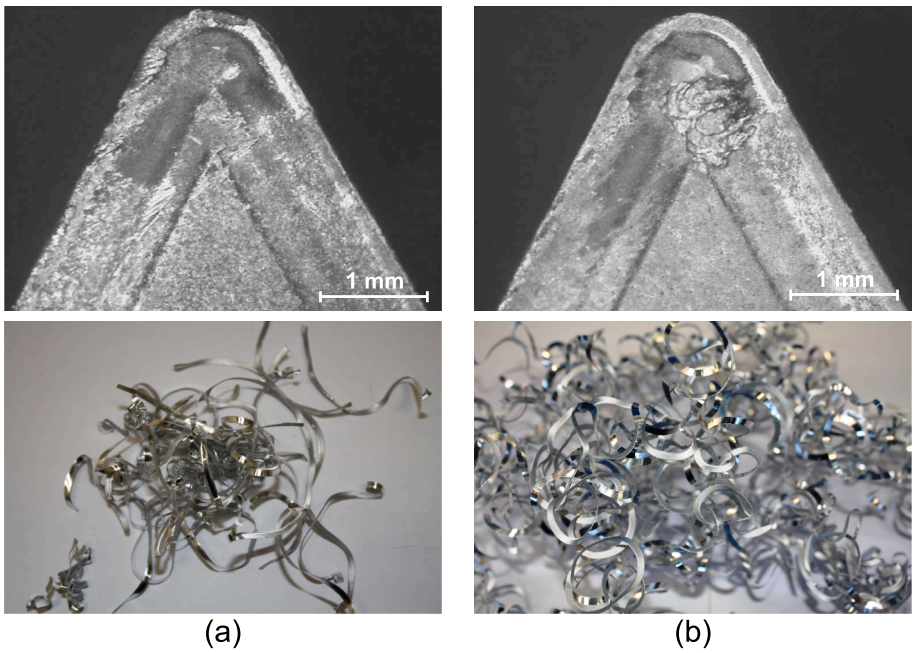

Fig. 7. Images of the tool rake face and the chip: a) v_c = 80 m/min; f = 0.05 mm/rev; b) v_c = 200 m/min; f = 0.20 mm/rev.

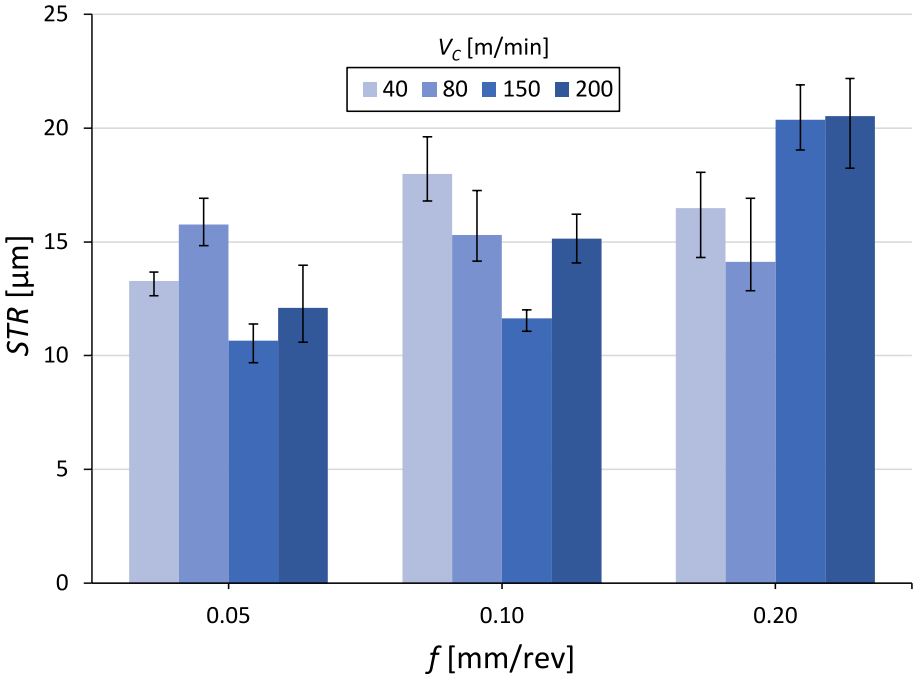

Fig. 8. Mean values of the straightness (*STR*) as a function of the feed rate (*f*), for each cutting speed (v_c).

The minimum and maximum values of *CRO* range from 3.74 µm (f = 0.05 mm/rev, v_c = 200 m/min) to 23.56 µm (f = 0.20 mm/rev, v_c = 200 m/min). For this geometrical deviation, f seems to be the most influential variable, regardless of v_c, showing a similar trend to *Ra*. It has been observed that *CRO* tends to increase as f increases. This increase is more pronounced between 0.10 and 0.20 mm/rev (approximately 40 %) than in the range of 0.05 to 0.10 mm/rev (almost doubled in some cases). In the case of v_c, the range of f between 0.05 and 0.10 mm/rev does not appear to be significantly affected. However, a more pronounced impact of this parameter is evident when the maximum f value (0.2 mm/rev) is applied, showing a tendency to increase *CRO* as v_c increases. Therefore, the combination of high f and v_c leads to the worst results. The combination of high vibrations at high f, together with the instability of the BUL and BUE at high v_c, leads to larger deviations of this variable.

Furthermore, there is a greater spread in the results than that shown by *STR*. As previously commented, BUL and BUE periodically detach, generating alterations in the cutting process (vibrations and instabilities). These alterations occur at specific moments during machining. The higher sensitivity of *CRO* with the cutting parameters, as well as its higher spread, may be related to the way both deviations are measured. Fig. 3 shows that *STR* is measured longitudinally, running through the entire profile created during machining, and averaging the results using a least squares adjustment. In contrast, *CRO* is measured in

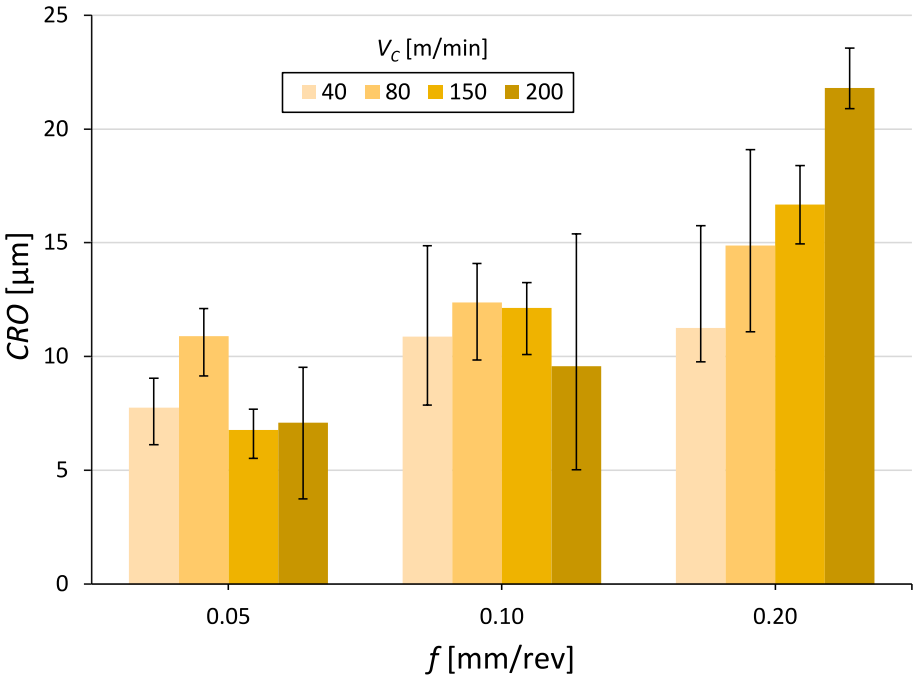

Fig. 9. Mean values of the circular runout (*CRO*) as a function of the feed rate (*f*), for each cutting speed (v_c).

specific sections of the profile, providing a snapshot of the machining process, which may result in greater oscillations [26]. The coincidence of the BUL/BUE detachment zone or of these instabilities with the *CRO* measurement point (transverse measurement) causes greater dispersion than in *STR* (averaged over the entire *L*). This occurs more clearly when high cutting and feed rates are combined (Fig. 7).

The trends described can be verified through an ANOVA analysis, which identifies the influence of input variables on the variability of output variables. The results obtained in the ANOVA analysis are presented in including DF (degree of freedom), *SS* (sum of squares), *F* and *P* (statistical parameters).

Table 4, including *DF* (degree of freedom), *SS* (sum of squares), *F* and *P* (statistical parameters).

The results indicate that both *f* and v_c have a statistically significant effect on *Ra*. However, *f* has a much greater impact, as evidenced by the magnitude of its *F-value* and the extremely low value of its *P-value*. For *STR*, *f* has a statistically significant effect with a very low *P-value*, while v_c shows no significant effect (*P-value* > 0.05). A similar trend to *Ra* is observed for *CRO*. In addition, the interaction *f*-v_c has a significant effect on all output variables. This suggests that the responses are influenced not only by the cutting parameters individually, but also by the interaction between them. The significant interaction effects indicate that the relationship between the input and output variables is not simply additive. In summary, it is crucial to analyse both effects and interactions when examining the impact of cutting conditions on the machined workpiece, particularly when high values are combined.

Table 4
ANOVA analysis.

Variable	Source	*DF*	*SS*	*F-Value*	*P-Value*
Ra	*f*	2	22.9545	284.59	<0.0001
	v_c	3	0.5304	4.38	0.0071
	Residual	66		–	–
	Interaction *f*-v_c	6	2.0083	30.73	<0.0001
STR	*f*	2	293.8806	23.53	<0.0001
	v_c	3	35.9835	1.92	0.1348 > 0.05
	Residual	66	412.1679	–	–
	Interaction *f*-v_c	6	345.0749	51.43	<0.0001
CRO	*f*	2	785.7675	50.48	<0.0001
	v_c	3	95.1063	4.07	0.0102
	Residual	66	513.7048	–	–
	Interaction *f*-v_c	6	345.1615	20.48	<0.0001

After the analysis, the experimental dataset was prepared to obtain a predictive model based on an artificial neural network, as shown in Fig. 5a. As outlined in the experimental methodology, the first step was to normalise (from 0 to 1) the input and output variables through Eq. (8), in order to improve the performance of the neural network, avoiding the problems of scale difference in each variable. The histograms with the distribution of the input and output normalised variables are shown in Fig. 10.

Fig. 11 plots *MSE* as a function of *N*, for training (*Tr*) and validation (*Val*), as well as the sum of the *MSE* obtained in both phases (*Total*). This error is also visible in the graph classified by the complete normalised dataset (*ALL*) or by the individual normalised variables (*Ra*, *STR* or *CRO*). As shown in Fig. 11, *MSE* exhibits underfitting when using a small number of neurons (between 1 and 5) and stabilizes from 5 neurons onwards. The minimum error occurs when using 8 neurons (N_{opt}). For a higher number of neurons (from 8 to 20), an asymptotic behaviour is observed without any overfitting.

Table 5 shows the numerical values for *MSE*. The normalised dataset had a value of 8.76×10^{-3}, which is low enough to ensure a good network fit. The output variable with the lowest value was *Ra* (5.29×10^{-3}), followed by *STR* (8.34×10^{-3}). The worst result was obtained for CRO (5.29×10^{-3}). This is due to the greater spread of this variable, for the reasons discussed above. Additionally, it is noted that the error during the training phase is either smaller or comparable to the error during the validation phase. This suggests that the data used for validation are representative of the experimental dataset.

Fig. 12a shows the training performance for the normalised dataset. The epochs (iterations) run were 32. The *MSE* decreased gradually during in training and validation, reaching a minimum value (0.003721) at epoch 26. In addition, the *MSE* in the validation phase was lower than in the training phase. Fig. 12b plots the ANN training error histogram. Approximately 90 % of the results indicate an error value of less than ± 0.1. About 8 % of the dataset shows an error between ± 0.1 and ± 0.2, while only 2 % of the data shows an error between ± 0.2 and ± 0.27.

The regression for the normalised variables in both the training and

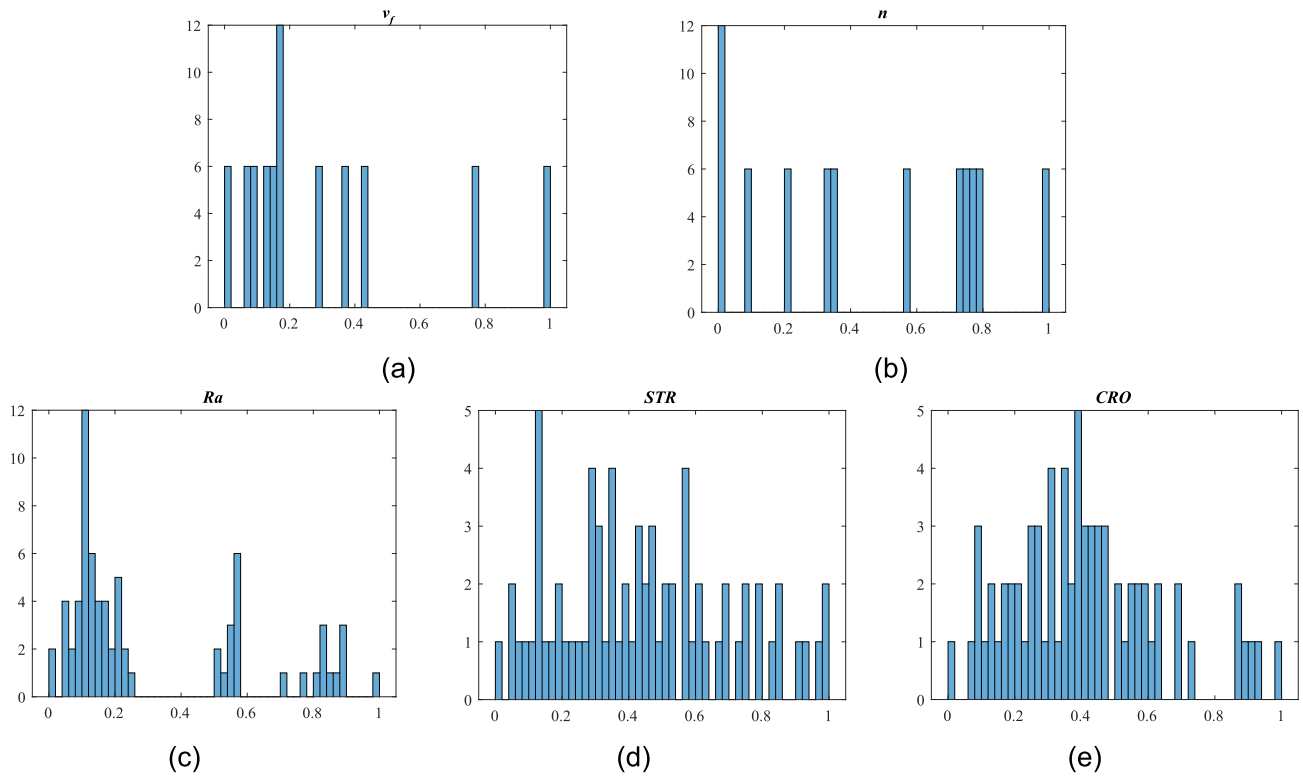

Fig. 10. Histograms for the normalised inputs and outputs variables: (a) Feed (v_f); (b) Rotational speed (n); (c) Arithmetic average of roughness profile (Ra); (d) Straightness (STR); (e) Circular runout (CRO).

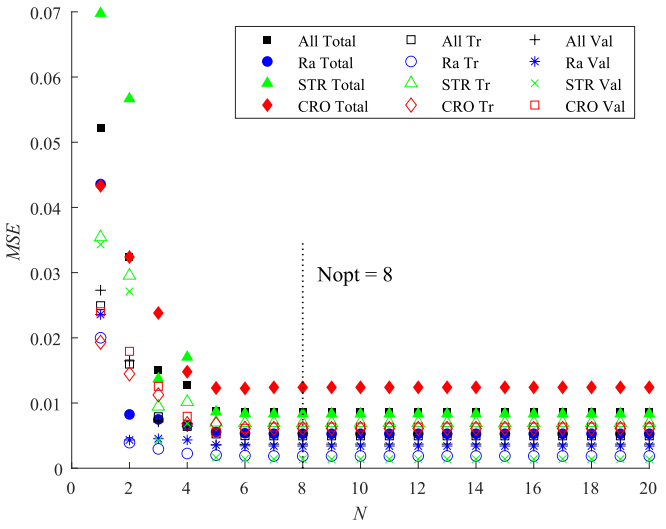

Fig. 11. Mean Square Error (MSE) as a function of the neurons number in the hidden layer (N).

Table 5
MSE for $N = 8$ in the training and validation phases, for the normalized dataset.

	MSE-Tr (x10^{-3})	***MSE-Val*** (x10^{-3})	***MSE-Total*** (***MSE-Tr*** + ***MSE-Val***) (x10^{-3})
Ra	3.41	1.88	5.29
STR	6.94	1.40	8.34
CRO	6.10	6.31	12.41
All dataset	5.04	3.72	8.76

validation phases, as well as for the entire dataset, are shown in Fig. 13. Table 6 displays *RMSE* and R^2 for the normalised dataset. Furthermore, a comparative analysis of the outcomes yielded by the three evaluated algorithms (LM, BR and SGC) is presented. As can be observed, despite the absence of a statistically significant difference, the LM algorithm is the one that yields the best result. Given that no overfitting was observed, the BR algorithm does not present a significant advantage. Conversely, given that the number of data processed is relatively limited, memory efficiency is not a significant concern, and therefore, SCG does not offer a notable improvement over LM. Therefore, the subsequent findings are derived from the implementation of the LM algorithm.

For the LM algorithm, the R^2 value in the training phase was 0.845, whereas its value was higher (0.920) in the validation phase. This behaviour is in good agreement with that shown by the *RMSE*. The R^2 for all dataset (training + validation) was 0.869. Thus, the implemented ANN achieved a reasonable fit by considering the three output variables (*Ra*, *STR*, and *CRO*) simultaneously.

Next, the results of the adjustment are analysed by considering each variable independently, after reversing the normalisation process of the data (Eq. (8). The regression results for each output variable, in the validation and training phases, and for all dataset, are displayed in Fig. 14. Table 7 shows the *RMSE* and R^2 for each variable.

The variable with the best fit was *Ra* ($R^2 = 0.973$), followed by *STR* ($R^2 = 0.906$). The worst results were obtained for *CRO* ($R^2 = 0.872$). Nevertheless, the fit level presented by all three variables can be considered satisfactory, considering other models found in the literature, as discussed below. This pattern is consistent across all three variables in training and validation. Therefore, the selected data samples for both phases are representative of the overall distribution of the dataset for each variable.

Fig. 15 shows the error histogram for the output variables. Regarding *Ra*, approximately 80 % of the data exhibits a deviation lower than 0.10 μm, with a maximum deviation of 0.369 μm. Approximately 85 % of *STR*

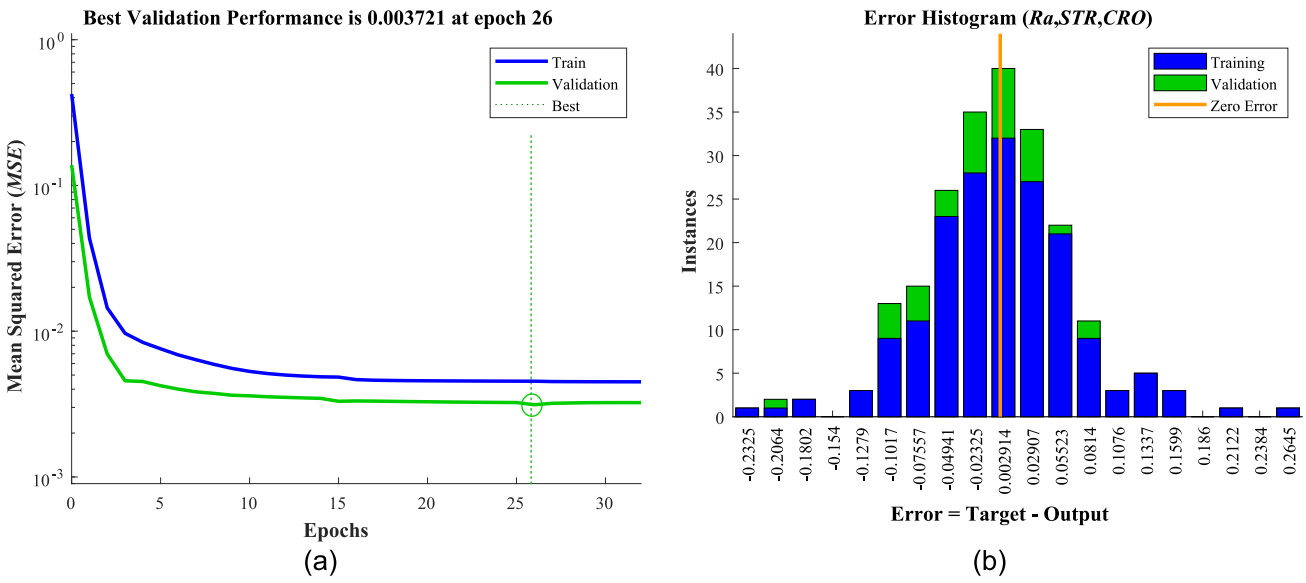

Fig. 12. (a) Training performance and (b) Training error histogram for the normalised dataset.

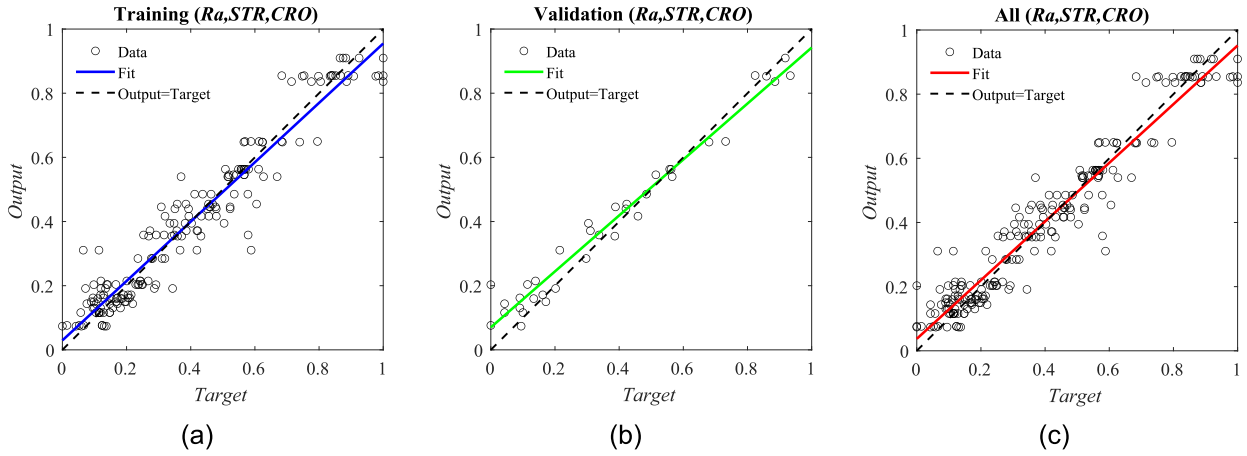

Fig. 13. Regression results: (a) Training data; (b) Validation data; (c) All dataset.

Table 6
RMSE and R^2 of the ANN ($N_{opt} = 8$).

		RMSE			***R²***		
	Algorithm	Training	Validation	All	Training	Validation	All
All dataset (normalised)	LM	0.071	0.061	0.069	0.845	0.920	0.860
	BR	0.070	0.060	0.068	0.838	0.909	0.853
	SCG	0.069	0.059	0.067	0.836	0.910	0.851

values show a deviation of less than 1.5 μm, with the maximum deviation being 2.6 μm. In terms of *CRO*, about 82 % of the data had a deviation lower than 2 μm, showing a maximum of 5.2 μm. These values appear reasonable given the magnitude of the analysed deviations.

These results can be compared with other regression models found in the literature review. The potential (Eq. (9) [23,27] and polynomial-potential models (Eq. (10) [20,22], are the most used. Additionally, non-linear exponential models are used for macrogeometrical deviations according to Eq. (11) [25,26].

$$GD = Kv_c^x f^y \tag{9}$$

$$GD = K_0 v_c^a f^b + c v_c^d + e f^g + h \tag{10}$$

$$GD = C_0 e^{\sum_{i=1}^{2}\sum_{j=1}^{2} K_{ij} f^i v_c^{yj}} \tag{11}$$

Where *GD* is the studied geometrical deviation, *K*, *x* and *y* are the parameters of the model in Eq. (9), K_0, *a*, *b*, *c*, *d*, *e*, *g* and *h* the parameters of the model in Eq.10, and C_0, K_{ij} and *y* the parameters of the model in Eq.11.

The experimental dataset from this work was used to obtain regressions using the indicated models. The software used to obtain the coefficients of the models was SPSS Statistics 29.0 (IBM, 2022). This software has linear and non-linear regression modules; the nonlinear regression procedure allows for fitting customised non-linear models, such as the exponential model in Eq. (10) and (11). For the potential model (Eq. (9) the equation has been linearised by applying logarithms.

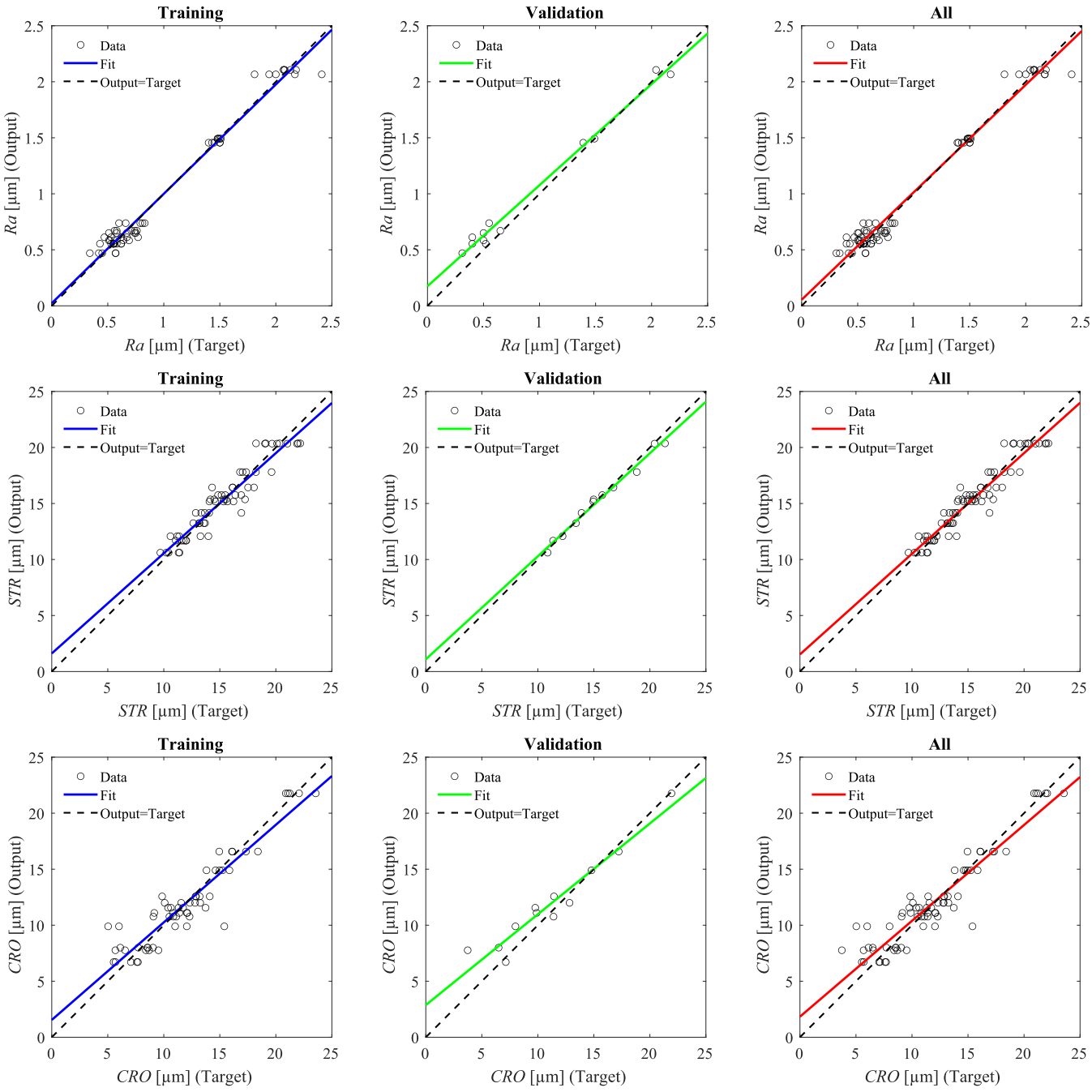

Fig. 14. Regression results for *Ra*, *STR* and *CRO*.

Table 7
RMSE and R^2 of the ANN ($N_{opt} = 8$), for each output variable.

	***RMSE* [µm]**			***R²***		
	Training	Validation	All	Training	Validation	All
Ra	0.091	0.123	0.097	0.976	0.956	0.973
STR	1.040	0.466	0.968	0.891	0.975	0.906
CRO	1.548	1.574	1.552	0.866	0.868	0.872

Once linearised, multiple linear regression has been applied to obtain the model coefficients [70]. Regarding the polynomial model (Eq. (10) the Levenberg-Marquardt algorithm has been used. It is an iterative algorithm used to solve non-linear least squares problems. It combines the gradient descent method with the Gauss-Newton method to improve convergence in complex models, especially when the functions are highly nonlinear or have multiple polynomial terms [71]. It is robust for models with multiple terms and is the default option in the SPSS 'Nonlinear Regression' procedure [71]. For the exponential model (Eq. (11) the form of the model has been specified in the 'Nonlinear Regression' dialog box function (SPSS), which allows to enter the exponential model expression in the form, and then uses the Levenberg-Marquardt algorithm to fit the parameters iteratively until the model converges to the best fit. To prevent the algorithm from getting trapped in local minima and convergence problems, initial seed values have been provided for the model coefficients [72].

The equations that result from the analysis are shown in Table 8. The adjusted coefficient of determination (R^2) expresses the model fit. In the potential models, the exponent of v_c (x) is much lower than the exponent of f (y) for all geometrical deviations. This suggests that f has a stronger influence than v_c. The influence is greatest in *Ra* ($y = 0.86$), reduced in

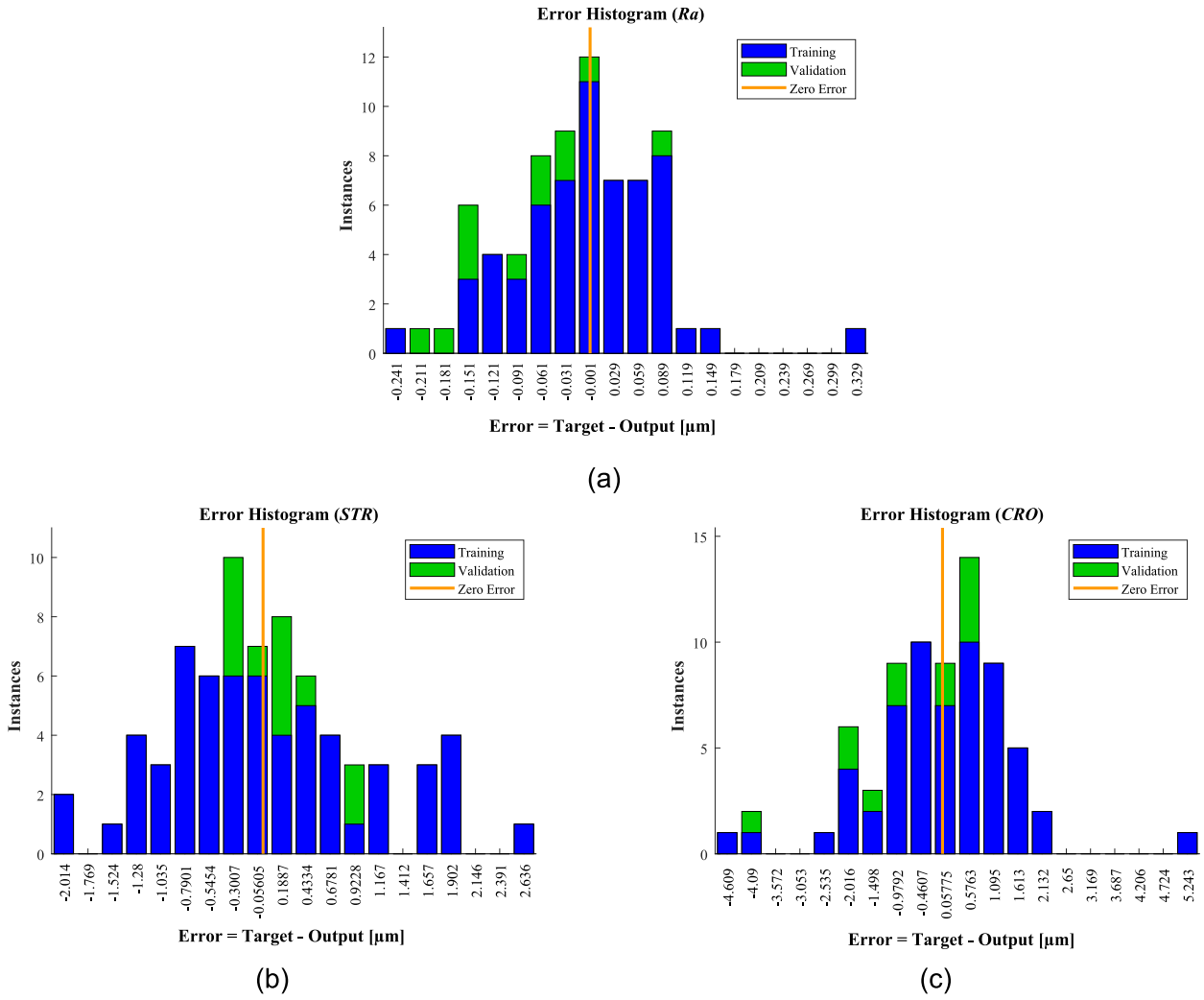

Fig. 15. Error histograms for a) *Ra*, b) *STR* and c) *CRO*.

Table 8
Regression models.

Model	Geometrical Deviation	Equation	R^2
Potential	*Ra*	$Ra = 7.96 v_c^{-0.06} f^{0.86}$	0.747
	STR	$STR = 30.64 v_c^{-0.04} f^{0.23}$	0.384
	CRO	$CRO = 27.49 v_c^{0.05} f^{0.50}$	0.538
polynomial-potential	*Ra*	$\log(Ra) = -0.7763 + 0.0009 v_c - 1.2319 f - 0.0265 v_c f + 49.3628 f^2$	0.911
	STR	$\log(STR) = 2.9283 - 0.0076 v_c + 1.2689 f + 0.0246 v_c f - 8.0903 f^2$	0.625
	CRO	$\log(CRO) = 1.8734 + 0.0014 v_c + 5.1571 f + 0.0386 v_c f - 20.3334 f^2$	0.702
Exponential	*STR*	$STR = 13.53 e^{(0.05 f^2 v_c)}$	0.415
	CRO	$CRO = 9.12 e^{(0.11 f^2 v_c)}$	0.699

CRO ($y = 0.50$), and much smaller for *STR* ($y = 0.23$). In all cases, the exponent y is positive, indicating an increase in geometrical deviation with f. The model presents a reasonable fit for *Ra* ($R^2 = 0.747$), but for *STR* and *CRO*, the level of fit is low ($R^2 = 0.384$ and 0.538, respectively). Regarding the polynomial-potential models, interpreting the influence of v_c and f is more challenging due to the changes of signs observed in the first and second-degree terms. However, the level of fit is higher than for the potential model, showing *Ra* a high fit ($R^2 = 0.911$) and *STR* and *CRO* a reasonable fit ($R^2 = 0.625$ and 0.702, respectively). Finally, the exponential model shows that both deviations (*STR* and *CRO*) have a quadratic exponent for f, while it is linear for v_c. This suggests that these deviations are more affected by f and tend to increase as f increases. The level of fit is reasonable for *CRO* ($R^2 = 0.699$), while it is low for *STR* ($R^2 = 0.415$).

When comparing the fits obtained in these models with that obtained for the ANN, it is evident that a better fit was achieved using ANN for all three deviations analysed ($R^2 = 0.872$–0.973), mainly in the case of *STR* and *CRO* (Table 7). This is evident from Fig. 16, which shows in all cases a better fit of the ANN predictions compared to the rest of the models, in the three variables analysed. Therefore, the use of ANN has been shown to be a valid tool for the prediction of the geometrical variables studied. Additionally, the use of ANN has the benefit of predicting all three variables simultaneously in a single model.

The developed ANN predictive model was implemented in a Simulink environment (Fig. 17). The input variables are entered into a block (Normalization) where the normalised v_f (v_f_N) and n (n_N) values are obtained. These normalised input values are then used to predict the normalised output variables (*Ra_N*, *STR_N* and *CRO_N*) in the next block (Function Fitting Neural Network). Finally, the prediction of the normalised output variables (*Ra*, *STR* and *CRO*) are obtained (denormalization blocks).

A set of additional machining tests were carried out to test the ANN under different combinations of cutting parameters, from those used during training and validation. Table 9 displays the combinations of f, v_c,

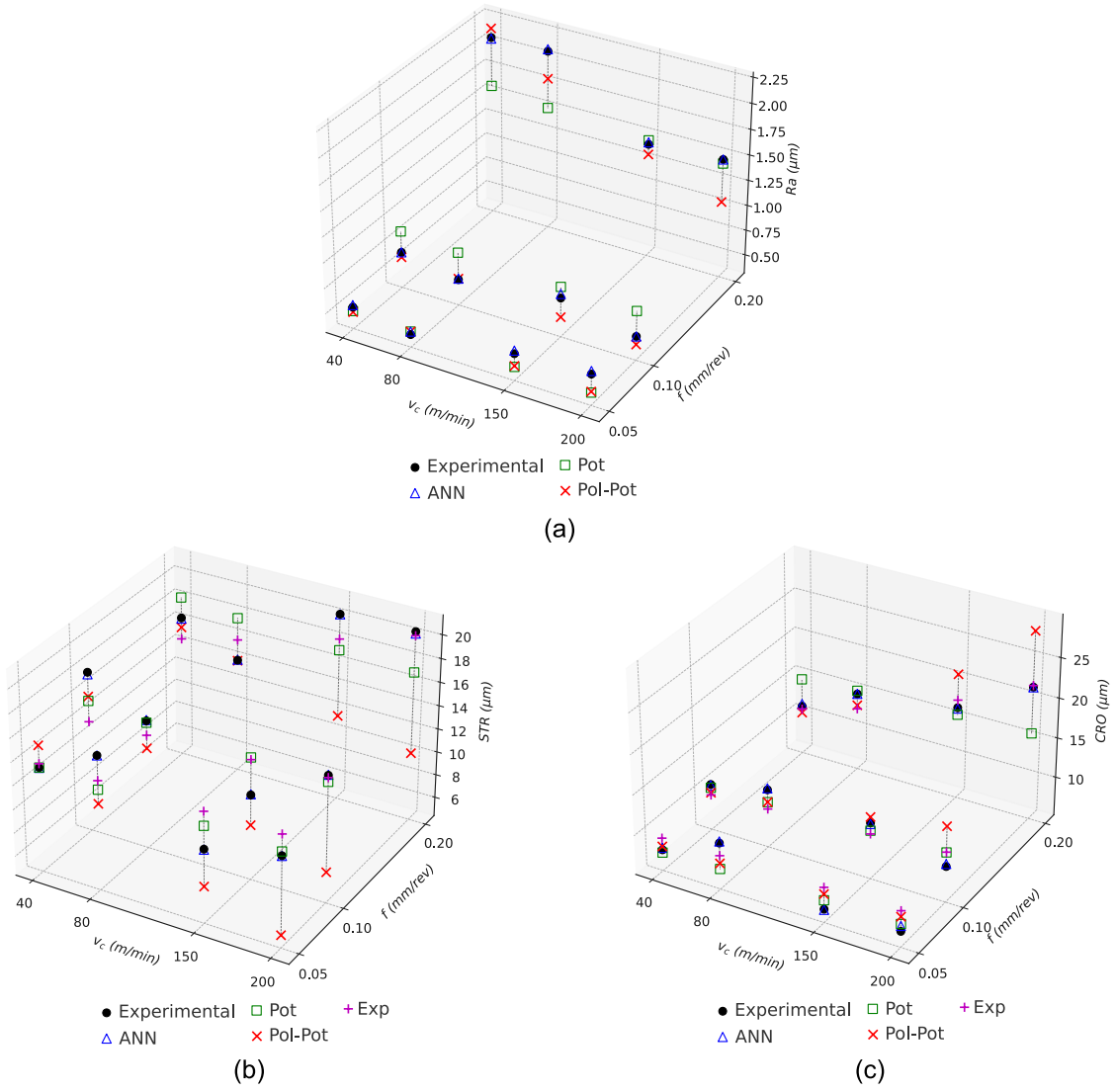

Fig. 16. Comparative experimental data (mean values) vs prediction models: a) *Ra*; b) Straightness (*STR*); c) Circular Runout (*CRO*).

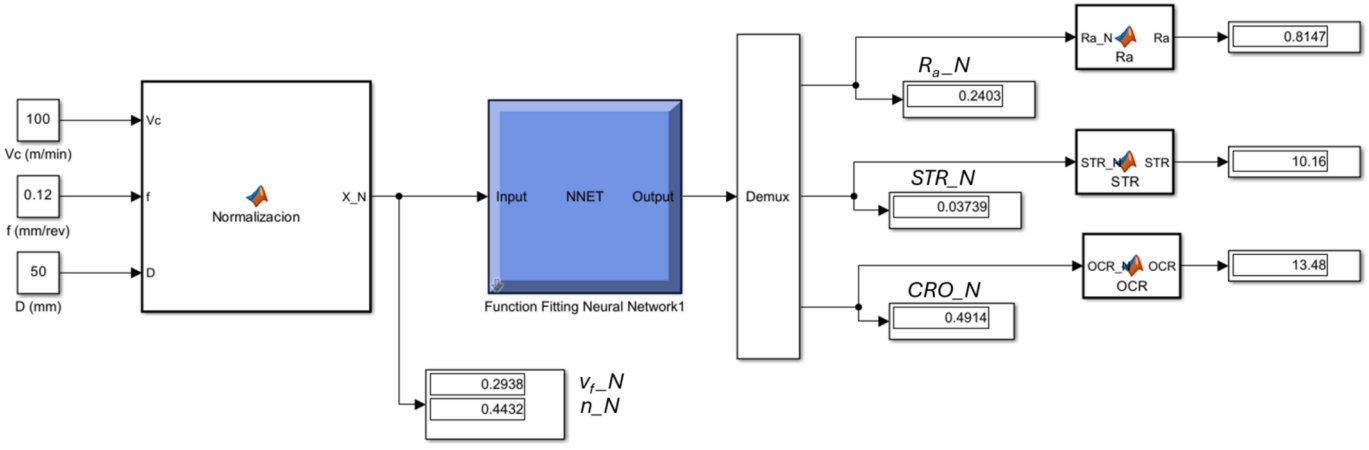

Fig. 17. ANN predictive model implemented in Simulink.

and *D* applied, along with the experimental results for the mean values of *Ra*, *STR*, and *CRO*. The table also shows the predicted values by the ANN, as well as the absolute and percentage difference between the target and the prediction.

Regarding *Ra*, the spread ranged from 0.36 to −0.10 μm, indicating a maximum deviation of approximately ± 10 %. For *STR*, the deviations oscillated between 3.14 and −2.31 μm, representing a maximum variation of about ± 25 %. Finally, *CRO* showed a maximum deviation from

Table 9
Dataset and results of the ANN testing phase.

v_c (m/min)	f (mm/r)	D (mm)	Ra (μm)	Ra_{ANN} (μm)	ΔRa (μm)	ΔRa (%)	STR (μm)	STR_{ANN} (μm)	ΔSTR (μm)	ΔSTR (%)	CRO(μm)	CRO_{ANN} (μm)	ΔCRO (μm)	ΔCRO (%)
100	0.12	50	0.76	0.81	−0.05	−6.58	13.3	10.16	3.14	23.61	11.45	13.48	−2.03	−17.73
60	0.07	40	0.52	0.48	0.04	7.69	19.4	16.35	3.05	15.72	10.12	12.04	−1.92	−18.97
175	0.15	50	0.91	1.01	−0.10	−10.99	15.98	17.48	−1.50	−9.39	17.30	19.11	−1.81	−10.46
225	0.25	50	4.15	3.79	0.36	8.67	26.12	28.43	−2.31	−8.84	42.80	40.45	2.35	5.49

2.35 to −2.03 μm, which represents a maximum oscillation of about ± 20 %. For *Ra*, the ANN predictions are consistently tight, regardless of the combination of cutting parameters used. However, for *STR* and *CRO*, the maximum variations in prediction occur at lower combinations of v_c and f (60 m/min and 0.07 mm/rev; 100 m/min and 0.12 mm/rev), while at higher combinations of v_c and f, the predictions are more precise (175 m/min and 0.15 mm/rev; 225 m/min and 0.25 mm/rev). It is important to acknowledge that the geometric deviations analysed show a high degree of dispersion, depending on the area of the part in which they are measured, as shown by the experimental results (Fig. 8 and Fig. 9). This variability is always present in the process itself and is difficult to eliminate, so prediction within these margins of error can be a good approximation to the real results obtained. While further enhancements to the models are possible, the incorporation of ANN has demonstrated an improvement in the predictive efficacy of the variables under examination when compared to existing models in the literature. Thus, the developed ANN model was shown to accurately determine micro and macro geometric deviations, in the proximity of the studied cutting parameter values and under the applied cutting conditions, making it a much more suitable procedure than the application of other regression models usually employed.

It should be noted that this work has a number of limitations, including its applicability to a single alloy and under the cutting conditions studied. Nevertheless, the demonstrated utility of neural networks in elucidating the interplay between variables at the micro and macrogeometric levels paves the way for novel avenues of inquiry and potential future actions. It would be beneficial to expand the number of data collected and the range of cutting parameters used, including the cutting depth. Furthermore, the inclusion of other microgeometrical variables of interest, such as *Rz* (Maximum height of the roughness profile) *Rsk* (Skewness of the roughness profile) and *Rku* (Kurtosis of the roughness profile), as well as parameters related to the profile spacing, such as *RSm* (Mean width of profile elements of the roughness profile), would be a valuable addition to the study. Regarding macrogeometrical deviations, it would be advantageous to include cylindricity (CYL), total radial oscillation (TRO), concentricity (CON) or coaxiality (COA), among others. In addition, the study should be expanded to cover other alloys of interest, such as AA92024 (Al-Cu) or Ti6Al4V. The demonstrated usefulness of ANNs suggests augmenting the number of output variables analysed (tool wear, cutting forces, cutting temperature, etc.). For this regard, it is recommended to explore more complex machine learning algorithms, such as deep learning, which can be used to accommodate the increased complexity of models when other variables are added.

4. Conclusions

This study investigated the influence of the cutting parameters (v_c and f) on various geometric deviations at micro and macro scale when turning in dry cylindrical parts of AA97075 aluminium alloy. Specifically, the arithmetical mean deviation of the roughness profile (*Ra*), straightness (*STR*) and circular runout (*CRO*) have been analysed. A predictive model of these deviations as a function of the input parameters has been obtained using artificial neural networks (ANN). The key findings are:

- The literature review reveals a lack of studies that apply artificial neural networks to obtain predictive models of macrogeometrical deviations in the dry machining of light alloys, despite the robustness and accuracy they have shown in the prediction of other output variables in this type of process.
- The study confirms that f has the most significant impact, particularly at higher feed rates. The increase in *Ra*, *STR*, and *CRO* with increased f highlights the sensitivity of surface quality and geometrical accuracy to this parameter. In contrast, v_c has a lesser but still significant impact compared to f. For all three analysed output variables, the optimal results are achieved by combining low f and high v_c.
- The ANOVA analysis reveals that *Ra*, *STR*, and *CRO* are influenced not only by f and v_c individually, but also by the interaction between them. The interaction effects are not simply additive and, therefore, it is crucial to analyse both effects simultaneously, particularly when high values are combined.
- The application of a shallow feedforward ANN has proven to be a robust tool for modelling and predicting *Ra*, *STR*, and *CRO* deviations based on cutting parameters. The proposed ANN model, trained and validated on an experimental dataset, achieved remarkable accuracy, as evidenced by reasonable adjusted R-squared (R^2) values (0.973 for *Ra*, 0.906 for *STR* and 0.872 for *CRO*), demonstrating its ability to capture the complexity of machining processes under the studied conditions.
- The performance of the ANN model was compared with traditional regression models (potential, polynomial-potential and exponential). While further enhancements to the models are possible, the ANN model consistently outperformed in terms of accuracy, providing a better fit to the experimental data for all output variables analysed. This highlights the advantage of ANNs in modelling complex manufacturing processes where parameter interactions can be non-linear and highly interdependent. Furthermore, the ANN model considers simultaneously geometrical variables at both the macro and micro scales.
- The testing of the ANN model with additional test data not included in the training set demonstrated the robustness of the model, confirming its practical usefulness for the pre-planning of machining parameters and the optimisation of surface quality and geometrical deviations under the studied cutting conditions.
- However, the study has a set of limitations and have potential for improvement, which suggests several potential areas for future research. These include expanding the ANN model to incorporate additional process input and output variables and cutting conditions; analysing various types of aluminum alloys; exploring advanced machine learning techniques and algorithms for even more accurate and adaptable modelling, among others.

CRediT authorship contribution statement

F.J. Trujillo: Writing – original draft, Software, Project administration, Methodology, Investigation, Formal analysis, Data curation, Conceptualization. **S. Martín-Béjar:** Writing – review & editing, Validation, Supervision, Methodology, Investigation. **F. Bañón:** Writing – review & editing, Validation, Supervision. **T. Andersson:** Writing – review & editing, Supervision, Formal analysis. **L. Sevilla:** Writing –

review & editing, Project administration, Methodology, Investigation, Formal analysis, Conceptualization.

Declaration of competing interest

The authors declare that they have no known competing financial interests or personal relationships that could have appeared to influence the work reported in this paper.

Acknowledgements

This work has received funding from the Ministerio de Ciencia e Innovación (Gobierno de España), through the research project "Expert system for improving surface integrity in sustainable machining of light alloys (SPAREMETAL)", with reference PID2021-125988OB-I00. The authors thank the Universidad de Málaga for their contribution to this work, which has received funding from the "II Plan Propio de Investigación, Transferencia y Divulgación Científica" of the Universidad de Málaga, through a grant for a research internship at the School of Engineering Science of the University of Skövde (Sweden). Funding for open access charge: Universidad de Málaga / CBUA.

Appendix A. Supplementary data

Supplementary data to this article can be found online at https://doi.org/10.1016/j.measurement.2024.116355.

Data availability

Data will be made available on request.

References

[1] Bagdi, Z.; Csámer, L.; Bakó, G. The Green Light for Air Transport: Sustainable Aviation at Present. *Cognitive Sustainability* **2023**, *2*, doi: 10.55343/COGSUST.55.
[2] Blanco, D.; Rubio, E.M.; Lorente-Pedreille, R.M.; Sáenz-Nuño, M.A. Sustainable Processes in Aluminium, Magnesium, and Titanium Alloys Applied to the Transport Sector: A Review. *Metals 2022, Vol. 12, Page 9* **2021**, *12*, 9, doi: 10.3390/MET12010009.
[3] P. Dwivedi, A.N. Siddiquee, S. Maheshwari, Issues and Requirements for Aluminum Alloys Used in Aircraft Components: State of the Art, *Russian Journal of Non-Ferrous Metals* 62 (2021) 212–225, https://doi.org/10.3103/S1067821221020048/TABLES/3.
[4] Shao, L.; Xue, N.; Li, W.; Liu, S.; Tu, Z.; Chen, Y.; Zhang, J.; Dai, S.; Liu, Q.; Shi, X.; et al. Effect of Cold-Spray Parameters on Surface Roughness, Thickness and Adhesion of Copper-Based Composite Coating on Aluminum Alloy 6061 T6 Substrate. *Processes 2023, Vol. 11, Page 959* **2023**, *11*, 959, doi: 10.3390/PR11030959.
[5] M.C. Santos, A.R. Machado, W.F. Sales, M.A.S. Barrozo, E.O. Ezugwu, Machining of Aluminum Alloys: A Review, *Int. J. Adv. Manuf. Technol.* 86 (2016) 3067–3080, https://doi.org/10.1007/s00170-016-8431-9.
[6] G.E. Totten, M.D. Scott, Handbook of Aluminum. (2003).
[7] E.A. Starke, J.T. Staley, Application of Modern Aluminum Alloys to Aircraft, *Prog. Aerosp. Sci.* 32 (1996) 131–172, https://doi.org/10.1016/0376-0421(95)00004-6.
[8] Ian Polmear, David St John, Jian-Feng Nie, M.Q. *Light Alloys; Section-2 Physical Metallurgy of Aluminium Alloys*; 2017; ISBN 9780080994314.
[9] C. Hodonou, M. Balazinski, M. Brochu, C. Mascle, Material-Design-Process Selection Methodology for Aircraft Structural Components: Application to Additive vs Subtractive Manufacturing Processes, *Int. J. Adv. Manuf. Technol.* 103 (2019) 1509–1517, https://doi.org/10.1007/S00170-019-03613-5/METRICS.
[10] Astakhov, V.P. Surface Integrity – Definition and Importance in Functional Performance. In *Surface Integrity in Machining*; Davim, J.P., Ed.; Springer London, 2010; pp. 1–35 ISBN 978-1-84882-873-5.
[11] Z. Liao, A. la Monaca, J. Murray, A. Speidel, D. Ushmaev, A. Clare, D. Axinte, R. M'Saoubi, Surface Integrity in Metal Machining - Part I: Fundamentals of Surface Characteristics and Formation Mechanisms, *Int J Mach Tools Manuf* 162 (2021) 103687, https://doi.org/10.1016/J.IJMACHTOOLS.2020.103687.
[12] Salguero, J.; Sol, I. Del; Gomez-Parra, A.; Batista, M. Machining of Al-Cu and Al-Zn Alloys for Aeronautical Components. *Advanced Aluminium Composites and Alloys* **2020**, doi: 10.5772/INTECHOPEN.93719.
[13] G.M. Krolczyk, R.W. Maruda, J.B. Krolczyk, S. Wojciechowski, M. Mia, P. Nieslony, G. Budzik, Ecological Trends in Machining as a Key Factor in Sustainable Production – A Review, *J Clean Prod* 218 (2019) 601–615.
[14] M. Nouari, B. Haddag, A. Moufki, S. Atlati, Investigation on the Built-up Edge Process When Dry Machining Aeronautical Aluminum Alloys, *Machining of Light Alloys* (2018) 35–48, https://doi.org/10.1201/B22153-2/INVESTIGATION-BUILT-EDGE-PROCESS-DRY-MACHINING-AERONAUTICAL-ALUMINUM-ALLOYS-MOHAMMED-NOUARI-BADIS-HADDAG-ABDELHADI-MOUFKI-SAMIR-ATLATI.
[15] F. Trujillo, L. Sevilla, M. Marcos, Experimental Parametric Model for Indirect Adhesion Wear Measurement in the Dry Turning of UNS A97075 (Al-Zn) Alloy, *Materials* 10 (2017) 152, https://doi.org/10.3390/ma10020152.
[16] Trujillo, F.J.; Sevilla, L.; Martín, F.; Bermudo, C. Analysis of the Chip Geometry in Dry Machining of Aeronautical Aluminum Alloys. *Applied Sciences (Switzerland)* **2017**, *7*, doi: 10.3390/app7020132.
[17] D. Carou, E.M. Rubio, J.P. Davim, Machinability of Magnesium and Its Alloys: A Review. (2015) 133–152, https://doi.org/10.1007/978-3-662-45088-8_5.
[18] J. Köhler, Machinability of Aluminum and Magnesium Alloys, *CIRP Encyclopedia of Production Engineering* (2014) 770–776, https://doi.org/10.1007/978-3-642-20617-7_6697.
[19] Martín-Béjar, S.; Trujillo, F.J.; Bermudo, C.; Sevilla, L. Fatigue Behavior Parametric Analysis of Dry Machined UNS A97075 Aluminum Alloy. *Metals 2020, Vol. 10, Page 631* **2020**, *10*, 631, doi: 10.3390/MET10050631.
[20] J. Salguero, F.J. Puerta, A. Gomez-Parra, F.J. Trujillo, L. Sevilla, M. Marcos, An Analysis of Geometrical Models for Evaluating the Influence of Feed Rate on the Roughness of Dry Turned UNS A92050 (Al-Cu-Li) Alloy, *Adv. Mater. Process. Technol.* (2016), https://doi.org/10.1080/2374068X.2016.1247333.
[21] F.J. Trujillo, L. Sevilla, J. Salguero, M. Batista, M. Marcos, Parametric Potential Model for Determining the Microgeometrical Deviations of Horizontally Dry-Turned UNS A97075 (Al-Zn) Alloy, *Adv Sci Lett* 19 (2013) 731–735, https://doi.org/10.1166/ASL.2013.4818.
[22] B. De Agustina, E.M. Rubio, M.Á. Sebastián, Surface Roughness Predictive Model of UNS A97075 Aluminum Pieces Obtained by Dry Turning Tests Based on the Cutting Forces, *Appl. Mech. Mater.* 217–219 (2012) 1628–1635, https://doi.org/10.4028/WWW.SCIENTIFIC.NET/AMM.217-219.1628.
[23] M.A. Sebastian, J.M. Sanchez-Sola, M.S. Carrilero, J.M. Gonzalez, M. Alvarez, M. Marcos, Parametric Model for Predicting Surface Finish of Machined UNS A92024 Alloy Bars, *Journal for Manufacturing Science and Production* 4 (2011) 181–188, https://doi.org/10.1515/IJMSP.2002.4.4.181.
[24] J.M. Sánchez, M.Á. Sebastián, E. Rubio, M. Sánchez-Carrilero, L.S. Hurtado, M. M. Bárcena, A Parametric Model for the Straightness Deviation in the Cutting Processes of Aluminum Alloys, *Mater. Sci. Forum* 526 (2006) 31–36, https://doi.org/10.4028/WWW.SCIENTIFIC.NET/MSF.526.31.
[25] J.M. Sánchez-Sola, M. Batista, J. Salguero, Á. Gómez, M. Marcos, Cutting Speed-Feed Based Parametric Model for Macro-Geometrical Deviations in the Dry Turning of UNS A92024 Al-Cu Alloys, *Key Eng Mater* 504–506 (2012) 1311–1316, https://doi.org/10.4028/WWW.SCIENTIFIC.NET/KEM.504-506.1311.
[26] F.J. Trujillo, L. Sevilla, M. Marcos, Cutting Speed-Feed Coupled Experimental Model for Geometric Deviations in the Dry Turning of UNS A97075 Al-Zn Alloys, *Adv. Mech. Eng.* 6 (2014) 382435, https://doi.org/10.1155/2014/382435.
[27] S. Martín Béjar, F.J. Trujillo Vilches, C. Bermudo Gamboa, L. Sevilla Hurtado, Parametric Analysis of Macro-Geometrical Deviations in Dry Turning of UNS A97075 (Al-Zn) Alloy, *Metals (basel)* 9 (2019) 1141, https://doi.org/10.3390/met9111141.
[28] D.-H. Kim, T. Kim, X. Wang, M. Kim, Y. Quan, J. Oh, S.-H. Min, H. Kim, B. Bhandari, I. Yang, et al., Smart Machining Process Using Machine Learning: A Review and Perspective on Machining Industry, *International Journal of Precision Engineering and Manufacturing-Green Technology* 5 (2018) 555–568, https://doi.org/10.1007/s40684-018-0057-y.
[29] Preez, A. du; Oosthuizen, G.A. Machine Learning in Cutting Processes as Enabler for Smart Sustainable Manufacturing. *Procedia Manuf* **2019**, *33*, 810–817, doi: 10.1016/J.PROMFG.2019.04.102.
[30] M. Gori, A. Betti, S. Melacci, *Machine Learning: A Constraint-Based Approach*, *Machine Learning: A Constraint-Based Approach* (2024) 1–537, https://doi.org/10.1016/C2020-0-03158-0.
[31] Ansari S.; Nassif, A.B. A Comprehensive Study of Regression Analysis and the Existing Techniques, *Advances in Science and Engineering Technology International Conferences*, ASET 2022 (2022) 2022, https://doi.org/10.1109/ASET53988.2022.9734973.
[32] Z. Jurkovic, G. Cukor, M. Brezocnik, T. Brajkovic, A Comparison of Machine Learning Methods for Cutting Parameters Prediction in High Speed Turning Process, *J Intell Manuf* 29 (2018), https://doi.org/10.1007/s10845-016-1206-1.
[33] V.C. Nguyen, D. Hoang Tien, V.H. Pham, T.D. Nguyen, Investigation and Optimization of Surface Roughness and Material Removal Rate in Face Finishing Milling of Ti-6Al-4V Under MQL Condition. *Lecture Notes, Mech. Eng.* 812–825 (2022), https://doi.org/10.1007/978-981-19-1968-8_68/TABLES/6.
[34] A.S. Rajesh, M.S. Prabhuswamy, S. Krishnasamy, Smart Manufacturing through Machine Learning: A Review, Perspective, and Future Directions to the Machining Industry, *J. Eng.* 2022 (2022) 9735862, https://doi.org/10.1155/2022/9735862.
[35] Aggogeri, F.; Pellegrini, N.; Tagliani, F.L. Recent Advances on Machine Learning Applications in Machining Processes. *Applied Sciences 2021, Vol. 11, Page 8764* **2021**, *11*, 8764, doi: 10.3390/APP11188764.
[36] Cherukuri, H.; Perez-Bernabeu, E.; Selles, M.; Schmitz, T. Machining Chatter Prediction Using a Data Learning Model. *Journal of Manufacturing and Materials Processing 2019, Vol. 3, Page 45* **2019**, *3*, 45, doi: 10.3390/JMMP3020045.
[37] C.H. Lee, J.S. Jwo, H.Y. Hsieh, C.S. Lin, An Intelligent System for Grinding Wheel Condition Monitoring Based on Machining Sound and Deep Learning, *IEEE Access* 8 (2020) 58279–58289, https://doi.org/10.1109/ACCESS.2020.2982800.
[38] M. Grzenda, A. Bustillo, Semi-Supervised Roughness Prediction with Partly Unlabeled Vibration Data Streams, *J Intell Manuf* 30 (2019) 933–945, https://doi.org/10.1007/S10845-018-1413-Z/TABLES/3.

[39] Lin, W.J.; Lo, S.H.; Young, H.T.; Hung, C.L. Evaluation of Deep Learning Neural Networks for Surface Roughness Prediction Using Vibration Signal Analysis. *Applied Sciences 2019, Vol. 9, Page 1462* **2019**, *9*, 1462, doi: 10.3390/APP9071462.
[40] A. Aljinović, B. Bilić, N. Gjeldum, M. Mladineo, Prediction of Surface Roughness and Power in Turning Process Using Response Surface Method and ANN, *Tehnicki Vjesnik* 28 (2021) 456–464, https://doi.org/10.17559/TV-20190522104029.
[41] P. Muñoz-Escalona, P.G. Maropoulos, Artificial Neural Networks for Surface Roughness Prediction When Face Milling Al 7075-T7351, *J Mater Eng Perform* 19 (2010) 185–193, https://doi.org/10.1007/S11665-009-9452-4.
[42] N. Fang, P.S. Pai, N. Edwards, Neural Network Modeling and Prediction of Surface Roughness in Machining Aluminum Alloys, *Journal of Computer and Communications* 04 (2016) 1–9, https://doi.org/10.4236/JCC.2016.45001.
[43] H.H.H. Al-Ani, Artificial Neural Network in the Prediction of Surface Roughness: A Comparative Study, *Sustainable Engineering and Innovation* 5 (2023) 141–150, https://doi.org/10.37868/SEI.V5I2.ID216.
[44] R. Kumar, S. Chauhan, Study on Surface Roughness Measurement for Turning of Al 7075/10/SiCp and Al 7075 Hybrid Composites by Using Response Surface Methodology (RSM) and Artificial Neural Networking (ANN), *Measurement (lond)* 65 (2015) 166–180, https://doi.org/10.1016/J.MEASUREMENT.2015.01.003.
[45] S. Arunkumar, N. Sriraman, R. Muraliraja, T. Vinod Kumar, V. Muthuraman, Performance Evolution in Machining Parameter of Al-Si (LM6) Alloy Using Neural Network, *Mater Today Proc* (2023), https://doi.org/10.1016/J.MATPR.2023.01.198.
[46] Kosarac, A.; Mladjenovic, C.; Zeljkovic, M.; Tabakovic, S.; Knezev, M. Neural-Network-Based Approaches for Optimization of Machining Parameters Using Small Dataset. *Materials 2022, Vol. 15, Page 700* **2022**, *15*, 700, doi: 10.3390/MA15030700.
[47] A. Eser, E. Aşkar Ayyildiz, M. Ayyildiz, F. Kara, Artificial Intelligence-Based Surface Roughness Estimation Modelling for Milling of AA6061 Alloy, *Adv. Mater. Sci. Eng.* 2021 (2021) 5576600, https://doi.org/10.1155/2021/5576600.
[48] N. Efkolidis, V. Dinopoulou, K. Kakoulis, Prediction of Cutting Forces in Drilling AL6082-T6 by Using Artificial Neural Networks. *IOP Conf Ser*, *Mater Sci Eng* 916 (2020), https://doi.org/10.1088/1757-899X/916/1/012036.
[49] H.T. Yau, P.H. Kuo, S.W. Hong, Milling Wear Prediction Using an Artificial Neural Network Model, *Eng Appl Artif Intell* 135 (2024) 108686, https://doi.org/10.1016/J.ENGAPPAI.2024.108686.
[50] Wiciak-Pikula, M.; Felusiak, A.; Twardowski, P. Artificial Neural Network Models for Tool Wear Prediction during Aluminium Matrix Composite Milling. *2020 IEEE International Workshop on Metrology for AeroSpace, MetroAeroSpace 2020 - Proceedings* **2020**, 255–259, doi: 10.1109/METROAEROSPACE48742.2020.9160064.
[51] V. Veeranaath, M. Nandana Mohanty, A. Kumar, P. Kumar, ANN Modeling of the Significance of Constraints in Turning Superalloys Using Coated PCBN Tools, *Mater Today Proc* 65 (2022) 20–28, https://doi.org/10.1016/J.MATPR.2022.03.559.
[52] P. Kulkarni, S. Chinchanikar, Modeling Turning Performance of Inconel 718 with Hybrid Nanofluid under MQL Using ANN and ANFIS, *Frattura Ed Integrità Strutturale* 18 (2024) 71–90, https://doi.org/10.3221/IGF-ESIS.70.04.
[53] K. Bousnina, A. Hamza, N. Ben Yahia, Predictive Optimization of Surface Quality, Cost, and Energy Consumption during Milling Alloy 2017A: An Approach Integrating GA-ANN and RSM Models, *Int. J. Interact. Des. Manuf.* 18 (2024) 5177–5196, https://doi.org/10.1007/S12008-023-01613-0/TABLES/13.
[54] K. Reza Kashyzadeh, S. Ghorbani, New Neural Network-Based Algorithm for Predicting Fatigue Life of Aluminum Alloys in Terms of Machining Parameters, *Eng Fail Anal* 146 (2023), https://doi.org/10.1016/J.ENGFAILANAL.2023.107128.
[55] Kalos, P.S.; Nandurkar, N.N.; Navale, L.G. Control of Roundness on Turned Cylindrical Bars Using Artificial Neural Network. *IEEM 2007: 2007 IEEE International Conference on Industrial Engineering and Engineering Management* **2007**, 597–601, doi: 10.1109/IEEM.2007.4419259.
[56] C. Du, C.L. Ho, J. Kaminski, Prediction of Product Roughness, Profile, and Roundness Using Machine Learning Techniques for a Hard Turning Process, *Adv Manuf* 9 (2021) 206–215, https://doi.org/10.1007/S40436-021-00345-2.
[57] J. Allen Jeffrey, S. Suresh Kumar, P. Vaidyaa, A. Nicho, A. Chrish, J. Joshith, Effect of Turning Parameters in Cylindricity and Circularity for O1 Steel Using ANN, *Mater Today Proc* 59 (2022) 1291–1294, https://doi.org/10.1016/J.MATPR.2021.11.518.
[58] Iso, *21920-2:2021 Geometrical Product Specifications (GPS) — Surface Texture: Profile — Part 2: Terms, Definitions and Surface Texture, Parameters* (2021).
[59] Iso, *1101:2017 Product Specifications (GPS)- Geometrical Tolerancing- Tolerances of Form, Orientation, Location and Run-out* (2017).
[60] V.K. Ojha, A. Abraham, V. Snášel, Metaheuristic Design of Feedforward Neural Networks: A Review of Two Decades of Research, *Eng Appl Artif Intell* 60 (2017) 97–116, https://doi.org/10.1016/J.ENGAPPAI.2017.01.013.
[61] F. Kamalov, S. Moussa, J.A. Reyes, Data Transformation in Machine Learning: Empirical Analysis, in: *2023 International Conference on Innovation and Intelligence for Informatics, Computing, and Technologies (3ICT)*, 2023, pp. 115–120, https://doi.org/10.1109/3ICT60104.2023.10391512.
[62] Oubaha, B.; Berrou, C.; Ji, X.; Nasser, Y.; Bidan, R. Le On Diversity in Discriminative Neural Networks. *ISIVC 2024 - Proceedings: 12th IEEE International Symposium on Signal, Image, Video, and Communications* **2024**, doi: 10.1109/ISIVC61350.2024.10577798.
[63] W. Li, R.C. Paffenroth, D. Berthiaume, Neural Network Ensembles: Theory, Training, and the Importance of Explicit Diversity. (2021).
[64] G. Lera, M. Pinzolas, Neighborhood Based Levenberg-Marquardt Algorithm for Neural Network Training, *IEEE Trans Neural Netw* 13 (2002) 1200–1203, https://doi.org/10.1109/TNN.2002.1031951.
[65] A. Gómez-Parra, M. Álvarez-Alcón, J. Salguero, M. Batista, M. Marcos, Analysis of the Evolution of the Built-Up Edge and Built-Up Layer Formation Mechanisms in the Dry Turning of Aeronautical Aluminium Alloys, *Wear* 302 (2013) 1209–1218, https://doi.org/10.1016/j.wear.2012.12.001.
[66] H. Gökkaya, The Effects of Machining Parameters on Cutting Forces, Surface Roughness, Built-Up Edge (BUE) and Built-Up Layer (BUL) during Machining AA2014 (T4) Alloy, *Journal of Mechanical Engineering* 56 (2010) 584–593.
[67] M.S. Carrilero, R. Bienvenido, J.M. Sánchez, M. Álvarez, A. González, M. Marcos, A SEM and EDS Insight into the BUL and BUE Differences in the Turning Processes of AA2024 Al–Cu Alloy, *Int J Mach Tools Manuf* 42 (2002) 215–220, https://doi.org/10.1016/s0890-6955(01)00112-2.
[68] Bethencourt, M.; Botana, F.J.; Calvino, J.J.; Carrilero, M.S.; Marcos, M. SEM and EDS Study of the BUL and BUE Formation in the Turning Processes of Aluminium-Cooper Alloys. In Proceedings of the Proceedings 14th International Congress on Electron Microscopy; Cancún (Méjico), 1998.
[69] F. Trujillo, S. Martín Béjar, C. Bermudo Gamboa, H. Manuel Jose, L. Sevilla, Influence of Tool Wear on Form Deviations in Dry Machining of UNS A97075 Alloy, *Metals (basel)* 11 (2021) 958, https://doi.org/10.3390/met11060958.
[70] C.C. Aggarwal, Linear Transformations and Linear Systems, *Linear Algebra and Optimization for Machine Learning* (2020) 41–95, https://doi.org/10.1007/978-3-030-40344-7_2.
[71] J.J. Moré, The Levenberg-Marquardt Algorithm: Implementation and Theory. (1978) 105–116, https://doi.org/10.1007/BFB0067700.
[72] IBM SPSS Regression 28 | Enhanced Reader (accessed on 6 November 2024).